

Computing a k -sparse n -length Discrete Fourier Transform using at most $4k$ samples and $O(k \log k)$ complexity

Sameer Pawar and Kannan Ramchandran

Dept. of Electrical Engineering and Computer Sciences

University of California, Berkeley

{spawar, kannanr}@eecs.berkeley.edu

Abstract

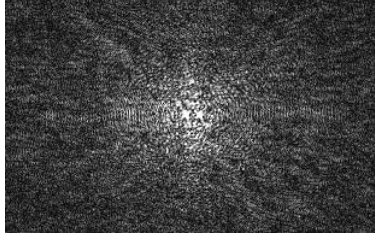
Given an n -length input signal \mathbf{x} , it is well known that its Discrete Fourier Transform (DFT), \mathbf{X} , can be computed in $O(n \log n)$ complexity using a Fast Fourier Transform (FFT). If the spectrum \mathbf{X} is exactly k -sparse (where $k \ll n$), can we do better? We show that asymptotically in k and n , when k is sub-linear in n (precisely, $k \propto n^\delta$ where $0 < \delta < 1$), and the support of the non-zero DFT coefficients is uniformly random, we can exploit this sparsity in two fundamental ways (i) **sample complexity**: we need only $M = rk$ deterministically chosen samples of the input signal \mathbf{x} (where $r < 4$ when $0 < \delta < 0.99$); and (ii) **computational complexity**: we can reliably compute the DFT \mathbf{X} using $O(k \log k)$ operations, where the constants in the big Oh are small and are related to the constants involved in computing a small number of DFTs of length approximately equal to the sparsity parameter k . Our algorithm succeeds with high probability, with the probability of failure vanishing to zero asymptotically in the number of samples acquired, M .

Our approach is based on filterless subsampling of the input signal \mathbf{x} using a small set of *carefully chosen uniform subsampling patterns guided by the Chinese Remainder Theorem (CRT)*. The idea is to cleverly exploit, rather than avoid, the resulting aliasing artifacts induced by this subsampling. Specifically, our subsampling operation on \mathbf{x} is designed to create aliasing patterns on the spectrum \mathbf{X} that “look like” parity-check constraints of good erasure-correcting sparse-graph codes. *We show how computing the sparse DFT \mathbf{X} is equivalent to decoding of these sparse-graph codes.* These codes further allow for fast peeling-style decoding, similar to that of fountain codes. The resulting DFT computation is low in both sample complexity and decoding complexity. We accordingly dub our algorithm the FFAST (Fast Fourier Aliasing-based Sparse Transform) algorithm. We analytically connect our proposed CRT-based aliasing framework to random sparse-graph codes, and analyze the performance of our algorithm using density evolution techniques from coding theory. Additionally our approach uncovers a new *deterministic* and efficient class of compressive sensing measurement matrices as an alternative to the popular choice of random matrices. Based on the qualitative nature of the subsampling patterns needed, our analysis is decomposed into two regimes: i) “very-sparse” ($0 < \delta \leq 1/3$), where $M < 2.5k$, and ii) “less-sparse” ($1/3 < \delta < 1$), where $M < 4k$ for $\delta < 0.99$.

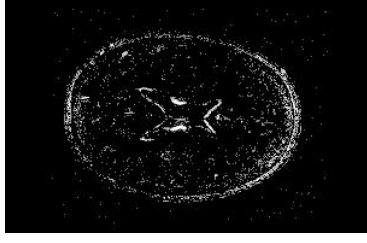
While our theory is asymptotic, our simulation results reveal that in practice our algorithm works even for moderate values of k and n , e.g. $k = 200$ and $n = 4080$. Further, when $k = 300$, and n is approximately 3.8 million, our algorithm achieves computational savings by a factor of more than 6000, and savings in the number of input samples by a factor of more than 3900 over the standard FFT. We analyze the 1-D DFT here, but our approach can be extended in a straightforward manner to multi-dimensional DFTs. Further, while our analysis is for the exactly sparse case, our approach can be extended to be robust to the more general approximately sparse and noisy measurement cases as well, albeit at the cost of increased sample and computational complexity. We provide extensive simulation results in Section VIII that corroborate our theoretical findings, and validate the empirical performance of the FFAST algorithm for a wide variety of 1D and 2D DFT settings for signals having an exactly or approximately sparse Fourier spectrum.

I. INTRODUCTION

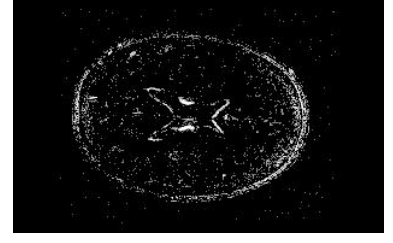
Spectral analysis using the Discrete Fourier Transform (DFT) has been of universal importance in engineering and scientific applications for a long time. The Fast Fourier Transform (FFT) is the fastest



(a) 2-D Fourier transform of a difference image between two consecutive axial slices of "Brain" MRI image.



(b) Exactly $k = 3250$ sparse $n = 195 \times 308$ dimensional differential Brain image.



(c) Perfectly reconstructed image using the FFAST algorithm from $M = 2.74k = 8910$ samples of the 2-D Fourier transform (Fig. 1(a)).

Fig. 1: An application of our FFAST algorithm to reconstruct the differentially sparse "Brain" image in an Magnetic Resonance Imaging (MRI) setting. In MRI, recall that samples are acquired in the Fourier domain, and the challenge is to speed up acquisition time by minimizing the number of samples needed to reconstruct the desired spatial domain image. a) Shows the spectrum of a difference image between two consecutive axial slices of the Brain. In MRI, samples are acquired in this domain. b) Shows the spatial domain differential Brain image of size $n = 195 \times 308$ with exactly $k = 3250$ non-zero pixels (sparsity is approximately 5%). The FFAST algorithm acquires less than 15% of the Fourier samples (sample complexity less than $3k$), and processes them using a low-complexity ($O(k \log k)$) FFAST algorithm to perfectly, up to machine precision, reconstruct it as shown in part (c).

known way to compute the DFT of an arbitrary n -length signal, and has a computational complexity¹ of $O(n \log n)$. Many applications of interest involve signals, e.g. relating to audio, image, and video data, seismic signals, biomedical signals, financial data, social graph data, cognitive radio applications, surveillance data, satellite imagery, etc., which have a sparse Fourier spectrum. In such cases, a small subset of the spectral components typically contain most or all of the signal energy, with most spectral components being either zero or negligibly small. If the n -length DFT, \mathbf{X} , of \mathbf{x} , is k -sparse, where $k \ll n$, can we do better in terms of both **sample** and **computational** complexity of computing the sparse DFT?

We answer this question affirmatively and show how to exploit the spectral domain sparsity to reduce the sample and computational complexity. As a motivating example, we have applied our proposed FFAST (Fast Fourier Aliasing-based Sparse Transform) algorithm to reconstructing the differentially sparse "Brain" image (see Fig. 1(b)) acquired in an Magnetic Resonance Imaging (MRI) application. In MRI, recall that samples are acquired in the Fourier domain, and the challenge is to speed up acquisition time by minimizing the number of samples needed to reconstruct the desired spatial domain image. We have an $n = 195 \times 308$ difference image of two consecutive axial slices of the Brain, as shown in Fig. 1(b), which is $k = 3250$ -sparse (i.e., approximately 5%-sparsity). Our algorithm synthesizes a big 195×308 size 2D-DFT using a smaller set of short 2D-DFTs of size 15×77 , 44×39 and 65×28 (two DFTs of each size) and successfully reconstructs the original image perfectly up to a machine precision, as shown in Fig. 1(c). The FFAST algorithm acquires only 14.84% of Fourier samples (see Fig. 1(a)), i.e. with a sample complexity of $M = 2.74k$.

This application leads to some interesting observations. First, while our theory is asymptotic in k and n , and targets the regime where k is sub-linear in n , in practice it applies even for moderate values where the sparsity is about 5%, as in the above MRI image example. Secondly, while our analysis is based on a uniformly random sparsity model, our algorithm seems applicable more generally to real-world

¹Recall that a single variable function $f(x)$ is said to be $O(g(x))$, if for a sufficiently large x the function $|f(x)|$ is bounded above by $|g(x)|$, i.e., $\lim_{x \rightarrow \infty} |f(x)| < c|g(x)|$ for some constant c . Similarly, $f(x) = \Omega(g(x))$ if $\lim_{x \rightarrow \infty} |f(x)| > c|g(x)|$ and $f(x) = o(g(x))$ if the growth rate of $|f(x)|$ as $x \rightarrow \infty$, is negligible as compared to that of $|g(x)|$, i.e. $\lim_{x \rightarrow \infty} |f(x)|/|g(x)| = 0$.

“clustered” sparsity settings, such as the MRI image of Fig 1(b).

The focus of this paper is however on 1-D signals having an exactly-sparse DFT. More precisely, our analysis focuses on the set of 1-D n -length signals \mathbf{x} whose n -point DFT, \mathbf{X} , has at most k non-zero coefficients that are uniformly randomly distributed. Our motivation for this focused study is three-fold: (i) to provide conceptual clarity of our proposed approach in a noiseless setting; (ii) to present our deterministic subsampling front-end measurement subsystem as a viable alternative to the class of randomized measurement matrices popular in the compressive sensing literature [1], [2]; and (iii) to explore the fundamental limits on both sample complexity and computational complexity for an exact-sparse DFT, which is of intellectual interest. This will allow us to address questions like: “Can we exploit the sparse structure of the DFT to be computationally more efficient than the $O(n \log n)$ FFT which applies more generally?” and “Can we make the sample and computational complexity *dependent only on k* ?”

The key insights derived from analyzing the exactly sparse signal model apply more broadly to the setting of approximately sparse signals (or where the measurements are further corrupted by noise). In Section VIII (see Figs. 14, 15(g)) we empirically validate the noise robustness of our proposed algorithm, under a Gaussian noise model for the tail coefficients, for settings involving an approximately sparse spectrum. However, unlike the exactly sparse case, for the noisy setting, the sample and the computational complexity of the FFAST algorithm are not $4k$ and $O(k \log k)$ any more. This is not surprising; as is well known in the literature, the measurement complexity for the noisy case is lower bounded by $\Omega(k \log(n/k))$ [3], [4]. While we provide empirical evidence of the noise robustness of our FFAST algorithm, we do not provide an analytical characterization of sample or computational complexity for such a noisy setting in this paper. Such an analysis is part of our ongoing and future work.

Our main theoretical result is that asymptotically in k and n , when k is sub-linear in n (precisely, $k \propto n^\delta$ where $0 < \delta < 1$), we can exploit the Fourier domain sparsity in two fundamental ways (i) **sample complexity**: we need to keep no more than rk samples of \mathbf{x} (where $r < 4$ when $0 < \delta < 0.99$ ²); and (ii) **computational complexity**: we can reliably compute the DFT \mathbf{X} using $O(k \log k)$ operations, where the constants in the big Oh are small and are related to the constants involved in computing a small number of DFTs of length approximately equal to the sparsity parameter k . Our algorithm succeeds with high probability, which we will use henceforth to mean, with probability at least $1 - O(1/M)$, where M is the sample complexity of the FFAST algorithm.

We emphasize the following caveats. First, as mentioned, our analytical results are probabilistic, and work asymptotically in k and n , with a success probability that approaches 1 asymptotically. This contrasts the $O(n \log n)$ FFT algorithm which works deterministically for all values of k and n . Secondly, in our $O(k \log k)$ computational complexity, we have not accounted for any I/O costs of reading and writing to/from memory, and assume the presence of random-access-memory. Thirdly, as mentioned, we assume a uniformly random model for the support of the non-zero DFT coefficients. Lastly, we require the signal length n to be a product of a few (typically 3 to 9) distinct primes³.

In effect, our algorithm trades off sample and computational complexity for asymptotically zero probability of failure guarantees in a non-adversarial sparsity setting, and is applicable whenever k is sub-linear in n (i.e. k is $o(n)$), but is obviously most attractive when k is much smaller than n . As a concrete example, when $k = 300$, and $n = 2^7 3^5 5^3 \approx 3.8 \times 10^6$, our algorithm achieves computational savings by a factor of more than 6000, and savings in the number of input samples by a factor of more than 3900 over the standard FFT (see [5] for computational complexity of a prime factor FFT

²Our analysis applies for any value of $0 < \delta < 1$. The sample complexity M will be no more than rk for some oversampling ratio r that increases as δ approaches 1 (the linear regime). For example, when $\delta = 0.999$, r is no more than 5, and for $\delta = 0.9999$, r is no more than 6. See Fig. 3 and Table II in Section III. The range from $0 < \delta < 0.99$ essentially covers the entire sub-linear sparsity regime of practical interest, and is therefore used as the default regime in the title of this paper.

³This is not a major restriction as in many problems of interest, the choice of n is available to the system designer, and choosing n to be a power of 2 is often invoked only to take advantage of the readily-available radix-2 FFT algorithms.

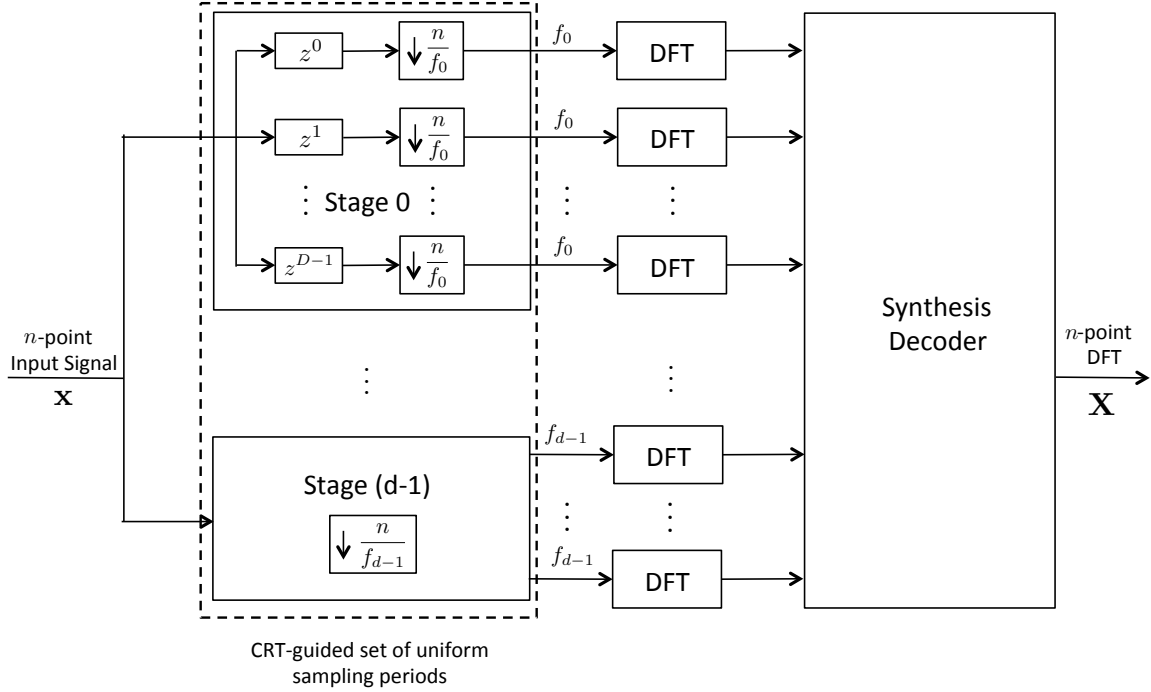


Fig. 2: Schematic block diagram of the FFAST architecture. The n -point input signal \mathbf{x} is uniformly subsampled by a carefully chosen set of patterns, guided by the Chinese-Remainder-Theorem, to obtain dD sub-streams. Each of the d stages has D sub-streams corresponding to the D delays. For the exactly sparse setting, $D = 2$. A sub-stream is of length approximately equal to the sparsity k , resulting in an aggregate number of samples $M = D \sum_{i=0}^{d-1} f_i \triangleq rk$, for a small constant r . Next, the (short) DFTs, of each of the resulting sub-streams are computed using an efficient FFT algorithm of choice. The big n -point DFT \mathbf{X} is then synthesized from the smaller DFTs using the peeling-like FFAST decoder. Although in this paper we focus on the low-complexity peeling-like FFAST decoder, in principle one can replace it with any decoder of choice that can synthesize the DFT \mathbf{X} from the smaller DFTs, e.g., a convex program like ℓ_1 -minimization. This can be particularly useful in settings when the DFT \mathbf{X} is approximately sparse or when the sampled data is corrupted by noise. Analysis of such an architecture is beyond the scope of this paper.

algorithm). This can be a significant advantage in many existing applications, as well as enable new classes of applications not thought practical so far.

Main Idea: At a high level, our algorithm uses a small and structured set of uniform subsampling operations applied directly on the input signal. It is well known from basic sampling theory that subsampling without anti-alias filtering creates spectral aliasing that destroys the original signal spectrum. Our key idea is to exploit rather than avoid this aliasing. This is done by recognizing that a *carefully designed subsampling operation will induce spectral aliasing artifacts that look like the parity constraints of good erasure-correcting codes that additionally have a fast peeling-decoding algorithm* (see Section IV-B for more details). As a result, both the sample complexity and the computational complexity of our algorithm are low.

Our main inspiration is drawn from the class of sparse graph-codes for erasure channels studied in coding theory, e.g., Low-Density-Parity-Check (LDPC) codes [6], fountain codes [7], [8], verification codes [9], etc. Why? These codes have two important properties that we would like to inherit: (a) they have very low computational complexity (iterative peeling-based) decoder; and (b) they are near-capacity achieving for the erasure channel. The first property bestows the desired low computational complexity, while the second property ensures that the sample complexity of the algorithm is near-optimal.

But how do we achieve this goal? We cannot induce any arbitrary code in the spectral domain

at our will as we can control only the subsampling operation on the time-domain signal. The key idea is to design subsampling patterns, guided by the *Chinese-Remainder-Theorem (CRT)*, that create the desired code-like aliasing patterns. As we will describe in Section V, the subsampling patterns are based on relatively co-prime integers for the very-sparse regime (sparsity-index $0 < \delta \leq 1/3$). When the spectrum is less-sparse ($1/3 < \delta < 1$), the subsampling patterns are a bit more complicated, comprising of “cyclically-shifted” overlapping co-prime integers. See Section VI for details.

Our approach is summarized in Fig. 2. As a concrete example, if the signal \mathbf{x} is of length $n \approx 10^6$ and its DFT \mathbf{X} has $k = 200$ non-zero coefficients, then the FFAST algorithm first generates 6 ($d = 3, D = 2$) uniformly sampled sub-streams of the input data, each of size ≈ 100 ($f_i \approx 100, i = 0, 1, 2$), and then synthesizes \mathbf{X} from the short DFTs of these 6 sub-streams. Due to the linear-time (in k) decoding complexity of the peeling-like FFAST decoder, our main computational bottleneck is in taking the small constant number of short (linear in k) DFTs. The precise number and the size of the short DFTs is quantified in Section III. For the entire range of practical interest of sub-linear sparsity (i.e. $k \propto n^\delta$ where $0 < \delta < 0.99$), the overall sample complexity of the FFAST algorithm is no more than $4k$, and the computational complexity is $O(k \log k)$ with small constants in the big-Oh. This is particularly gratifying because both the sample complexity and the computational complexity depend only on the sparsity parameter k , which is sub-linear in n .

Related Work: The problem of computing a sparse discrete Fourier transform of a signal is related to the rich literature of frequency estimation [10]–[13] in statistical signal processing as well as to compressive-sensing [1], [2]. In frequency estimation, it is assumed that a signal consists of k complex exponentials in the presence of noise and the focus is on ‘super-resolution’ spectral estimation techniques based on well-studied statistical methods like MUSIC and ESPRIT [10]–[13]. The methods used are based on subspace decomposition principles. In contrast, we take a different approach combining tools from coding theory, number theory, graph theory and signal processing. In compressive sensing, the objective is to reliably reconstruct the sparse signal from as few measurements as possible, using a fast recovery technique. The bulk of this literature concentrates on random linear measurements, followed by either convex programming or greedy pursuit reconstruction algorithms [2], [14], [15]. An alternative approach, in the context of sampling a continuous time signal with a finite rate of innovation is explored in [16]–[19]. Unlike the compressive sensing problem, where the resources to be optimized are the number of measurements⁴ (each measurement can further be a linear combination of multiple input samples) and the recovery cost, in our problem, we want to minimize the *number of input samples* (i.e., sample complexity) processed by an algorithm in addition to the recovery cost.

At a higher level though, despite some key differences in our approach to the problem of computing a sparse DFT, our problem is indeed closely related to the spectral estimation and compressive sensing literature, and our approach is naturally inspired by this, and draws from the rich set of tools offered by this literature.

A number of previous works [20]–[24] have addressed the problem of computing a 1-D DFT of a discrete-time signal that has a sparse Fourier spectrum, in sub-linear sample and time complexity. Most of these algorithms achieve a sub-linear time performance by first isolating the non-zero DFT coefficients into different bins, using specific filters or windows that have ‘good’ (concentrated) support in both, time and frequency. The non-zero DFT coefficients are then recovered iteratively, one at a time. The filters or windows used for the binning operation are typically of length $O(k \log(n))$. As a result, the sample and computational complexity is typically $O(k \log(n))$ or more. Moreover the constants involved in the big-Oh notation can be large, e.g., the empirical evaluation of [21] presented in [25] shows that for $n = 2^{22}$ and $k = 7000$, the number of samples required are $M \approx 2^{21} = 300k$ which

⁴Consider a compressive sensing problem with a measurement matrix A , i.e., $\mathbf{y} = A\mathbf{x}$, where \mathbf{y} is a measurement vector and \mathbf{x} is the input signal. Then, the sample complexity is equal to the number of non-zero columns of A and the measurement complexity is equal to the number of non-zero rows of A .

is 75 times more than the sample complexity $4k$ of the FFAST algorithm⁵. The work of [22] provides an excellent tutorial on some of the key ideas used by most sub-linear time sparse FFT algorithms in the literature. While we were writing this paper, we became aware of a recent work [26], in which the authors consider the problem of computing a noisy as well as an exactly-sparse 2-D DFT of size $\sqrt{n} \times \sqrt{n}$ signal. For an exactly sparse signal, and when $k = \sqrt{n}$, the algorithm in [26] uses $O(k)$ samples to compute the 2-D DFT of the signal in $O(k \log(k))$ time with a constant probability of failure (that is controllable but that does not appear go to zero asymptotically). In [27], the author proposes a sub-linear time algorithm with a sample complexity of $O(k \log^4 n)$ or $O(k^2 \log^4 n)$ and computational complexity of $O(k \log^5 n)$ or $O(k^2 \log^4 n)$ to compute a sparse DFT, with high probability or zero-error respectively. The algorithm in [27] exploits the Chinese-Remainder-Theorem, along with $O(\text{poly}(\log n))$ number of subsampling patterns to identify the locations of the non-zero DFT coefficients. In contrast, the FFAST algorithm exploits the CRT to induce ‘good’ sparse-graph codes using a small constant number of subsampling patterns and computes the sparse DFT with a vanishing probability of failure.

In summary, to the best of our knowledge, the FFAST algorithm is the first that we are aware of to compute an exactly k -sparse n -point DFT that has all of the following features:

- it has $O(k)$ sample complexity and $O(k \log k)$ computational complexity;
- it covers the *entire* sub-linear regime ($k \propto n^\delta$, $0 < \delta < 1$);
- it has a probability of failure that vanishes to zero asymptotically;
- it features the novel use of the Chinese Remainder Theorem to guide the design of a small deterministic set of uniform subsampling patterns that induce good sparse-graph channel codes.

The rest of the paper is organized as follows. Section II states the problem and introduces the notations. Section III presents our main results, and states the main theorem. Section IV exemplifies the mapping of computing the DFT to decoding over an appropriate sparse-graph code, and also provides review of the relevant background information on sampling, aliasing, and decoding on bipartite graphs. Sections V and VI provide the performance analysis of the FFAST algorithm for the *very-sparse* and the *less-sparse* regimes respectively, and can be bridged by a reader more interested in the practical aspects of our algorithm. Section VIII provides extensive simulation results that corroborate our theoretical findings, and validate the empirical performance of the FFAST algorithm for a wide variety of 1D and 2D DFT settings for signals having an exactly or approximately sparse Fourier spectrum.

II. PROBLEM FORMULATION, NOTATIONS AND PRELIMINARIES

A. Problem formulation

Consider an n -length discrete-time signal \mathbf{x} that is the sum of $k \ll n$ complex exponentials, i.e., its n -length discrete Fourier transform has k non-zero coefficients:

$$x[p] = \sum_{q=0}^{k-1} a_q e^{2\pi i \omega_q p/n}, \quad p = 0, 1, \dots, n-1, \quad (1)$$

where the discrete frequencies $\omega_q \in \{0, 1, \dots, n-1\}$ and the amplitudes $a_q \in \mathbb{C}$, for $q = 0, 1, \dots, k-1$. We consider the problem of identifying the k unknown frequencies ω_q and the corresponding complex amplitudes a_q from the time domain samples \mathbf{x} . A straightforward solution is to compute an n -length DFT, \mathbf{X} , using a standard FFT algorithm [28], and locate the k non-zero coefficients. Such an algorithm uses n samples and $O(n \log n)$ computations. When the DFT \mathbf{X} is known to be exactly k -sparse and $k \ll n$, computing all the n DFT coefficients seems redundant.

⁵As mentioned earlier, the FFAST algorithm requires the length of the signal n to be a product of a few distinct primes. Hence, the comparison is for an equivalent $n \approx 2^{22}$ and $k = 7000$.

In this paper, we address the problem of designing an algorithm, to compute the k -sparse n -point DFT of \mathbf{x} for the asymptotic regime of k and n , when the support of the non-zero DFT coefficients is uniformly random. We would like the algorithm to have the following features:

- it takes as few input samples M of \mathbf{x} as possible.
- it has a low computational cost that is a function of only the number of samples M .
- it is applicable for the entire sub-linear regime, i.e., for all $0 < \delta < 1$, where $k = O(n^\delta)$.
- it computes the DFT \mathbf{X} with a probability of failure vanishing to 0 as M becomes large.

In the next section, we setup the notations and provide definitions of the important parameters used in the rest of the paper.

B. Notation and preliminaries

Notation	Description
n	Ambient dimension of the signal \mathbf{x} .
k	Number of non-zero coefficients in the DFT \mathbf{X} .
δ	Sparsity-index: $k \propto n^\delta$, $0 < \delta < 1$.
M	Sample complexity: Number of samples of \mathbf{x} used by the FFAST algorithm to compute the DFT \mathbf{X} .
$r = M/k$	Oversampling ratio: Number of samples per non-zero DFT coefficient.
d	Number of stages in the “sub-sampling front end” of the FFAST architecture.
D	Number of sub-streams of the input signal \mathbf{x} generated in each stage of the “sub-sampling front end” of the FFAST architecture.
f_i	Number of samples of \mathbf{x} per sub-stream, in the i^{th} stage of the “sub-sampling front end” of the FFAST architecture; $M = \sum_{i=0}^{d-1} D f_i$.

TABLE I: Glossary of important notations and definitions used in the rest of the paper. The last three parameters are related to the “sub-sampling front end” of the proposed FFAST architecture (see Figure 4 for details).

Modulo-operator: For integers a, N , we use $(a)_N$ to denote the operation, $a \bmod N$, i.e., $(a)_N \triangleq a \bmod N$.

We now describe the Chinese-Remainder-Theorem (CRT) which plays an important role in our proposed FFAST architecture as well as in the FFAST decoder.

Theorem 1 (Chinese-Remainder-Theorem [28]). *Suppose n_0, n_1, \dots, n_{d-1} are pairwise co-prime positive integers and $N = \prod_{i=0}^{d-1} n_i$. Then, every integer ‘ a ’ between 0 and $N - 1$ is uniquely represented by the sequence r_0, r_1, \dots, r_{d-1} of its remainders modulo n_0, \dots, n_{d-1} respectively and vice-versa.*

Further, given a sequence of remainders r_0, r_1, \dots, r_{d-1} , where $0 \leq r_i < n_i$, Gauss’s algorithm can be used to find an integer ‘ a ’, such that,

$$(a)_{n_i} \equiv r_i \quad \text{for } i = 0, 1, \dots, d - 1. \quad (2)$$

For example, consider the following pairwise co-prime integers $n_0 = 3, n_1 = 4$ and $n_2 = 5$. Then, given a sequence of remainders $r_0 = 2, r_1 = 2, r_2 = 3$, there exists a unique integer ‘ a ’, such that,

$$\begin{aligned} 2 &\equiv a \bmod 3 \\ 2 &\equiv a \bmod 4 \\ 3 &\equiv a \bmod 5 \end{aligned} \quad (3)$$

It is easy to verify that $a = 38$ satisfies the congruencies in (3). Further, $a = 38$ is a unique integer modulo $N = n_0 n_1 n_2 = 60$ that solves (3).

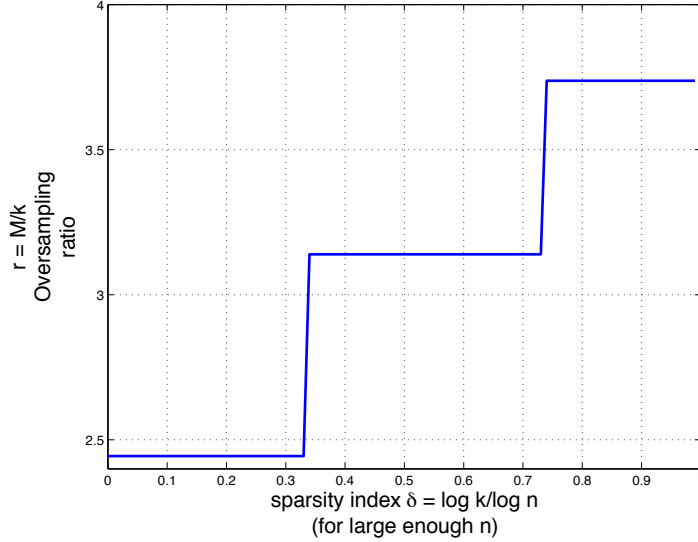


Fig. 3: Phase transition plot for the FFAST algorithm. The plot shows the relation between the oversampling ratio $r = M/k$, and the sparsity index δ for $0 < \delta < 0.99$, where $k \propto n^\delta$. The FFAST algorithm successfully computes the k -sparse n -point DFT \mathbf{X} of the desired n -point signal \mathbf{x} with high probability, as long as the number of samples M is above the threshold given in the plot. Note that for nearly the entire sub-linear regime of practical interest, e.g. $k < n^{0.99}$, the oversampling ratio $r < 4$. For asymptotic values of k , the oversampling ratio $r = 2d\eta$, where d is the number of stages in the FFAST architecture and η is the average number of samples per sub-stream normalized by the number of non-zero coefficients k . In Section V-D, we show that the number of stages d used in the FFAST architecture increases as δ approaches 1. The above phase transition plot is then obtained by using the constructions in Section V-D and the values of $d\eta$ from Table IV in Section V-C1.

III. MAIN RESULTS

We propose a novel FFAST algorithm to compute the (exactly) k -sparse n -point DFT, \mathbf{X} , of an n -point signal \mathbf{x} . In this paper, an n -length input signal \mathbf{x} is defined to have a k -sparse DFT \mathbf{X} , if \mathbf{X} has *at most* k non-zero arbitrary-valued coefficients, whose locations are uniformly randomly distributed in $\{0, 1, \dots, n-1\}$. The FFAST algorithm computes the k -sparse n -point DFT with high probability, using as few as $O(k)$ samples of \mathbf{x} and $O(k \log k)$ computations. The following theorem states the main result of the paper.

Theorem 2. *For any value of the sparsity index $0 < \delta < 1$, and n large enough, there exists a FFAST algorithm with parameters (n, k, M) , where $k = O(n^\delta)$, such that the FFAST algorithm can compute a k -sparse DFT \mathbf{X} of an n -length input \mathbf{x} with the following properties:*

- 1) **Sample complexity:** *The algorithm needs M samples of \mathbf{x} , where M can be as small as rk , where the oversampling ratio $r > 1$ is a small constant that depends on the sparsity index δ ;*
- 2) **Computational complexity:** *The computational complexity is $cM \log(M)$, where the constant c is small and related to the constants associated with computing a few approximately- M -length FFTs⁶.*
- 3) **Probability of success:** *The probability that the algorithm will correctly compute the k -sparse DFT \mathbf{X} is at least $1 - O(1/M)$.*

⁶Note that when $M = rk$, the computational complexity is $O(k \log k)$.

Proof: We prove the theorem in three parts. In Section V, we analyze the performance of the FFAST algorithm for the very-sparse regime ($0 < \delta \leq 1/3$), and in Section VI we analyze the less-sparse regime $1/3 < \delta < 1$. Lastly, in Section VII we analyze the sample and computational complexity of the FFAST algorithm. ■

Remark 3. [Oversampling ratio r] The minimum achievable oversampling ratio r of the sample complexity $M = rk$ depends on the number of stages d used in the FFAST architecture. The number of stages d , in turn, is a function of the sparsity index δ (recall $k \propto n^\delta$), and increases as $\delta \rightarrow 1$ (i.e., as the number of the non-zero coefficients, k , approach the linear regime in n). In Sections V and VI, we show how the number of stages d increases as δ approaches 1. Table II provides some example values of r and d for different values of the sparsity index δ . In Fig. 3 we plot r as a function of δ for a sparsity regime of practical interest, i.e., $0 < \delta < 0.99$.

δ	1/3	2/3	0.99	0.999	0.9999
d	3	6	8	11	14
r	2.45	3.14	3.74	4.64	5.51

TABLE II: The table shows the number of subsampling stages d used in the FFAST architecture, and the corresponding values of the oversampling ratio r (for different values of the sparsity index δ).

IV. FAST FOURIER TRANSFORM USING DECODING ON SPARSE-GRAPHS

In this section we describe our (deterministic) sub-sampling “front-end” architecture as well as the associated FFAST decoding “back-end” algorithm for computing the k -sparse n -point DFT, and we will connect this to the framework of decoding over sparse-graph codes. Before we delve into the details, we first review two background concepts from signal processing. We will use simple examples. Consider a 20-point discrete-time signal $\mathbf{x} = (x[0], \dots, x[19])$ whose 20-point DFT \mathbf{X} is 5-sparse. Let the 5 non-zero DFT coefficients of \mathbf{x} be $X[1] = 1, X[3] = 4, X[5] = 1, X[10] = 3$ and $X[13] = 7$.

- 1) **Aliasing:** If a signal is subsampled in the time domain, its frequency components mix together, i.e., alias, in a pattern that depends on the sampling procedure. For example, consider uniform subsampling of \mathbf{x} by a factor of 5 (see Fig. 4) to get $\mathbf{x}_s = (x[0], x[5], x[10], x[15])$. Then, the 4-point DFT of \mathbf{x}_s is⁷:

$$\begin{aligned}
X_s[0] &= X[0] + X[4] + X[8] + X[12] + X[16] = 0 \\
X_s[1] &= X[1] + X[5] + X[9] + X[13] + X[17] = 9 \\
X_s[2] &= X[2] + X[6] + X[10] + X[14] + X[18] = 3 \\
X_s[3] &= X[3] + X[7] + X[11] + X[15] + X[19] = 4
\end{aligned}$$

In general if the sampling period is N (we assume that N divides n) then

$$X_s[i] = \sum_{j \equiv (i)_{n/N}} X[j], \quad (4)$$

where the notation $(i)_{n/N}$ denotes the operation $i \bmod n/N$.

⁷Subsampling is usually followed by a scaling gain equal to the subsampling factor, e.g., when a signal is subsampled by 5 a scaling gain of 5 is applied to all the samples. In this paper we assume this to be an inherent operation of subsampling, and we will not carry around this gain explicitly.

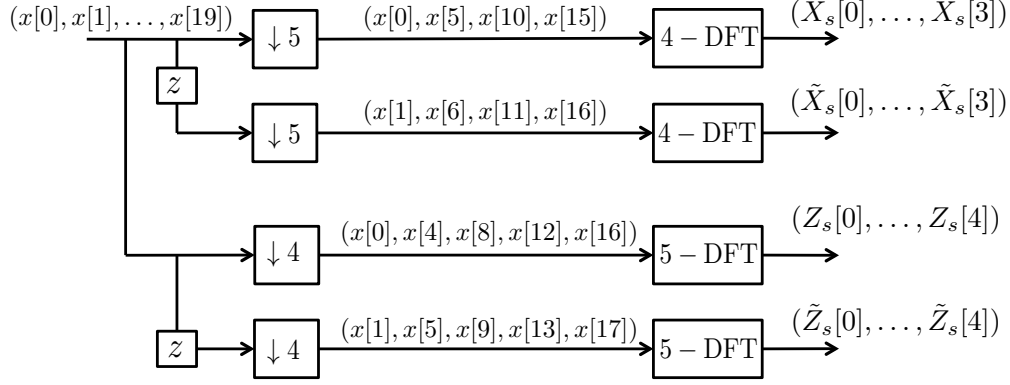


Fig. 4: A toy-example of the front end sub-sampling architecture of the FFAST algorithm. The input to the FFAST architecture is a 20-point discrete-time signal $\mathbf{x} = (x[0], \dots, x[19])$. The input signal and its unit delayed version are first subsampled by 5 to obtain two sub-streams ($D = 2$), each of length $f_0 = 4$. A 4-point DFT of each sub-stream is then computed to obtain the observations $(X_s[\cdot], \tilde{X}_s[\cdot])$. Similarly, downsampling by 4 followed by a 5-point DFT provides the second set of $f_1 = 5$ observations $(Z_s[\cdot], \tilde{Z}_s[\cdot])$. Note that the number of samples per sub-stream f_0 and f_1 in the two different stages ($d = 2$) are pairwise co-prime and are factors of $n = 20$. In general, the choice of subsampling factors depend on the sparsity index δ . For the very-sparse regime, ($0 < \delta \leq 1/3$), the subsampling factors are such that the number of samples per sub-stream in the different stages of the FFAST architecture are relatively co-prime factors of n (see Section V for details). For the less-sparse regime, ($1/3 < \delta < 1$), the number of samples per sub-stream in different stages have a more complicated “cyclically-shifted” overlapping co-prime structure (see Section VI for details).

- 2) **Shift in time:** From elementary Discrete Fourier Transform properties, we know that a circular shift in the time domain results in a phase shift in the frequency domain. Consider a circularly shifted sequence $\mathbf{x}^{(1)}$ obtained from \mathbf{x} as $x^{(1)}[i] = x[(i + 1)_n]$. The DFT coefficients of the shifted sequence are given as, $X^{(1)}[j] = \omega_n^j X[j]$, where $\omega_n = \exp(2\pi i/n)$ is an n^{th} root of unity. In general a circular shift of n_0 results in $X^{(n_0)}[j] = \omega_n^{jn_0} X[j]$.

A. Computing a sparse DFT is equivalent to decoding on a sparse-graph

Using the above 20-point example, we explain how to compute the k -sparse n -point DFT of a signal, using decoding over sparse graphs. Let, the input signal \mathbf{x} be processed through the front-end of the FFAST architecture, shown in Fig. 4, to obtain the observations $(X_s[\cdot], \tilde{X}_s[\cdot])$ and $(Z_s[\cdot], \tilde{Z}_s[\cdot])$.

For now, we focus only on the paths that produce the outputs $X_s[\cdot]$ and $Z_s[\cdot]$. Figures 5(a), 5(c) and 5(e) show the magnitude plots of the discrete-time signal \mathbf{x} and its subsampled versions, while Figures 5(b), 5(d) and 5(f) show the magnitude plots of the corresponding DFTs of appropriate lengths. Note that the observation $X_s[1]$ is a combination of three non-zero DFT coefficients of \mathbf{x} , we refer to such observations as “multi-tons”. Likewise the observations that consists of exactly one non-zero DFT coefficient of \mathbf{x} are referred to as “singletons”, e.g. $X_s[2]$, while the ones that consists of all the zero DFT coefficients are called “zero-tons”, e.g., $X_s[0]$ or $Z_s[2]$. Consider first that a “genie” informs us which observations are singletons, as well as, the location and value of the contributing non-zero DFT coefficient. We will later explain (in Section IV-C) how to get rid of the genie. Then, the FFAST algorithm can recover the DFT coefficients $X[1], X[3]$ and $X[10]$. After, subtracting the contribution of these uncovered DFT coefficients from the observations, more singleton observations are created. Thus, with the help of the genie, the FFAST algorithm can potentially recover all the 5 non-zero DFT coefficients of \mathbf{x} via an iterative peeling procedure.

An alternative and more convenient way to analyze this peeling procedure is to first represent the observations in the form of a bi-partite graph (see Fig. 6) where the left (variable) nodes correspond

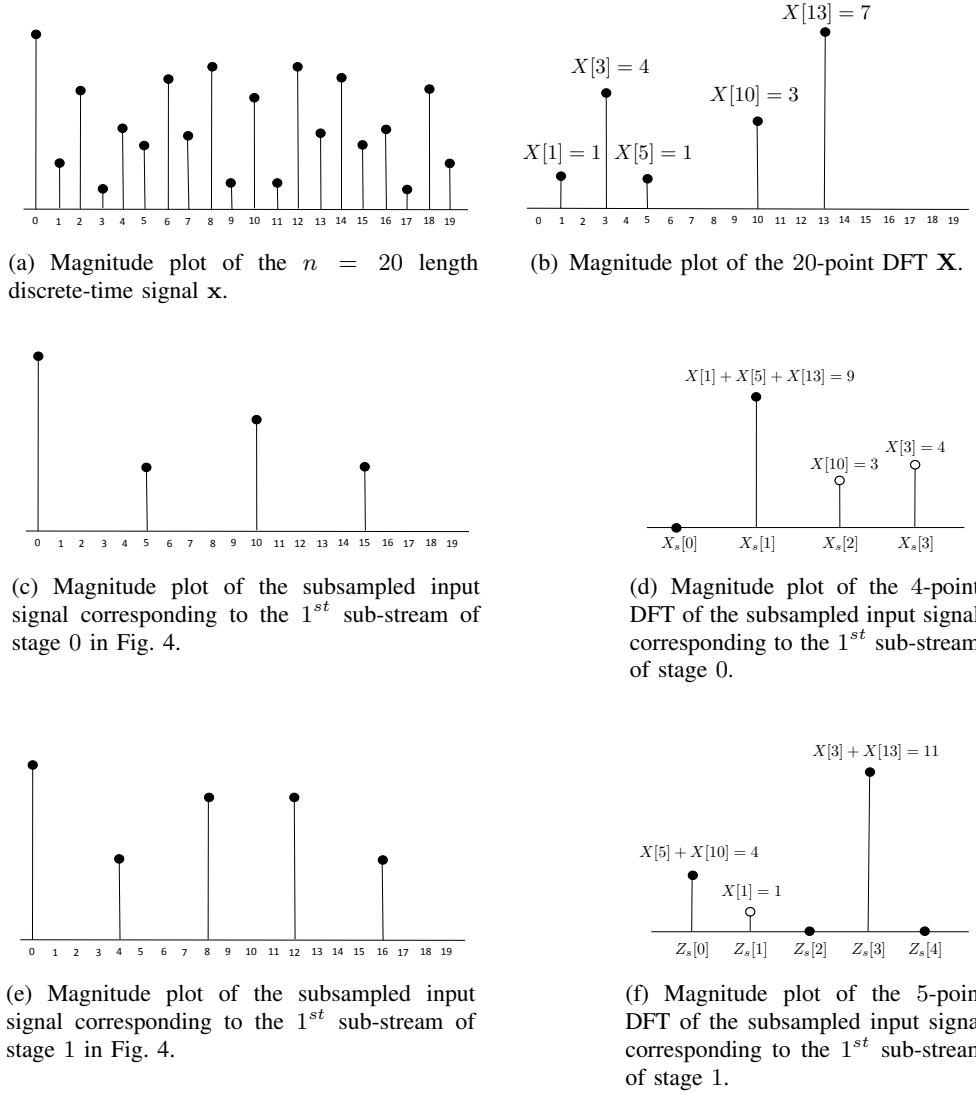


Fig. 5: Frequency aliasing induced by the FFAST architecture for the 20-point toy example signal \mathbf{x} . The left hand side sub-figures (a), (c), (e) are the magnitude plots of the time-domain signals \mathbf{x} and the 1st sub-streams in each of the two stages respectively. The sub-figures (b), (d), (f) on right, provide the magnitude plots of the DFT of respective time-domain signals on the left. Note that the observations $X_s[2]$, $X_s[3]$ and $Z_s[1]$ are singletons (marked by ‘unfilled circles’), $X_s[1]$, $Z_s[0]$ and $Z_s[3]$ are multi-tons, and $X_s[0]$, $Z_s[2]$ and $Z_s[4]$ are zero-tons.

to the non-zero DFT coefficients of \mathbf{x} (unknown and to be computed) and the right (check) nodes correspond to the observations generated through the FFAST architecture of Fig. 4. A check node with an edge degree 1 corresponds to a singleton observation, while the ones having the edge degrees equal to 0 and greater than 1 correspond to zero-ton and multi-ton observations respectively. Iterative-decoding on the graph given in Fig. 6 can be used to compute the DFT of \mathbf{x} from the observations.

Thus, the FFAST architecture has *transformed the problem of computing the DFT of \mathbf{x} into that of decoding over a sparse bi-partite graph* of Fig. 6.

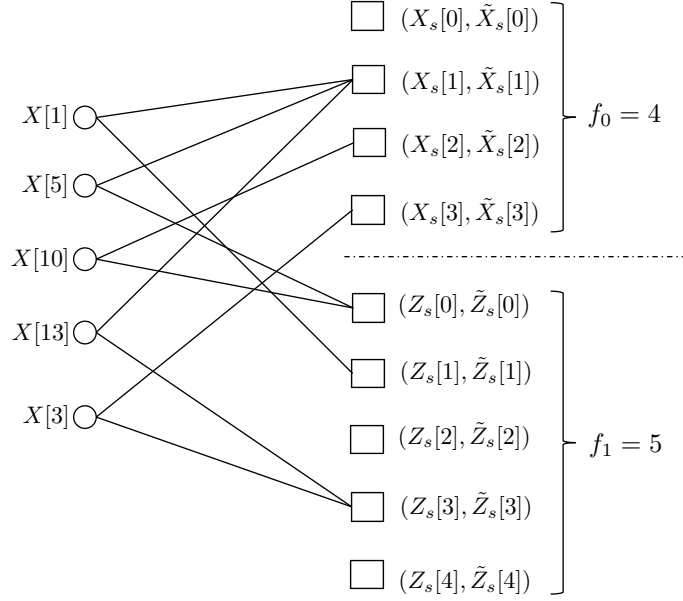


Fig. 6: A 2-left regular degree bi-partite graph representing the relation between the unknown DFT coefficients and the observations obtained through the FFAST architecture shown in Fig. 4, for the 20-point example signal \mathbf{x} . Variable (left) nodes correspond to the DFT coefficients and the check (right) nodes are the observations. The observation at each check node is a 2-dimensional complex-valued vector.

Erasure Channel	Sparse DFT
1. Explicitly designed sparse-graph code.	1. Implicitly designed sparse-graph code induced by sub-sampling.
2. $n - k$ correctly received packets.	2. $n - k$ zero DFT coefficients.
3. k -erased packets.	3. k unknown non-zero DFT coefficients
4. Peeling-decoder recovers the values of the erased packets using ‘singleton’ check nodes. The locations of which packets are erased are <i>known</i> .	4. Peeling-decoder recovers <i>both</i> the values and the locations of the non-zero DFT coefficients using ‘singleton’ check nodes. The locations of the non-zero DFT coefficients are <i>not known</i> . This results in a $2\times$ cost (i.e., $D = 2$) in the sample complexity.
5. Codes based on regular-degree bipartite graphs are near-capacity-achieving. More efficient, capacity-achieving irregular-degree bipartite graph codes can be designed.	5. The FFAST architecture based on uniform subsampling can induce only left-regular degree bi-partite graphs.

TABLE III: Comparison between decoding over a sparse-graph code for a packet erasure channel and computing a sparse DFT using the FFAST architecture.

B. Connection to coding for packet erasure channels

The problem of decoding over sparse bi-partite graphs has been well studied in the coding theory literature. In this section we draw an analogy between decoding over sparse-graph codes for a packet erasure channel and decoding over bi-partite graphs induced by the FFAST architecture.

Consider an $(n, n - m)$ packet erasure code. Each n -length codeword consists of $(n - m)$ information packets and m parity packets. Suppose that the code is used over an erasure channel that uniformly at random drops some k number of packets. A bi-partite graph representation of the parity check matrix of the code, after subtracting the contribution of the correctly received packets, is shown in Fig. 7(a). In Table III we provide comparison between decoding over bi-partite graphs of Fig. 7(a) and Fig. 7(b).

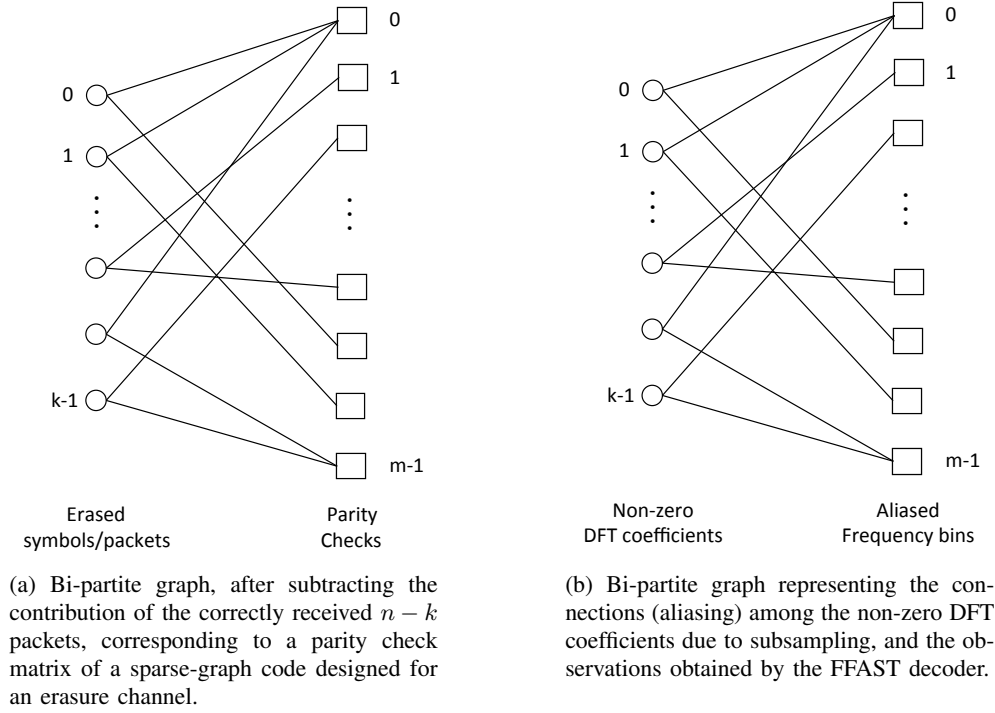


Fig. 7: Comparison between the bi-partite graphs corresponding to the parity check matrix of a sparse-graph code for an erasure channel and a graph induced by the FFAST architecture.

Thus, the problem of decoding over bi-partite graphs induced by the FFAST architecture is closely related to the decoding of sparse-graph codes for an erasure-channel. We use this analogy: a) to design a set of uniform sub-sampling patterns that induce ‘good’ left-regular degree sparse-graph codes; and b) to formally connect our proposed Chinese-Remainder-Theorem based aliasing framework to random sparse-graph codes constructed using a balls-and-bins model, and analyze the convergence behavior of our algorithm using density evolution techniques.

C. FFAST Decoder

In Section IV-A we described an iterative peeling-decoder to compute the sparse DFT \mathbf{X} for a toy example with the help of a “genie” that informed the decoder if a check node is a zero-ton, singleton or multi-ton, as well as, the location of the corresponding non-zero DFT coefficient in case of a singleton check node. In this section, we show how to get rid of the “genie” by using the additional observations $\tilde{X}_s[\cdot]$ and $\tilde{Z}_s[\cdot]$. The resulting iterative decoding algorithm is referred to as the ‘FFAST-decoder’. First, we make the following important observation: if a check node is a singleton, then by computing the phase of the ratio of its observations, e.g., $\frac{n}{2\pi} \angle(\tilde{X}_s[2]/X_s[2]) = 10$, we can identify the index of the non-zero DFT coefficient, 10 in this example, connected to this check node and the first observation, $X_s[2] = 3$, provides the value of the non-zero DFT coefficient. In general, as shown in [29], identifying the support or the location of a non-zero DFT coefficient connected to a singleton check node from multiple (two in this example) observations is equivalent to the problem of estimating the frequency of a single sinusoid from its time domain samples. The problem of estimating a single sinusoid from noiseless or noisy time domain samples goes back to the signal processing literature from several decades ago, and the ratio test discussed above is a special case of well-known techniques used in [10] and [30] for a similar problem.

In particular, this has been used in [29] to show that by having two⁸ observations per check node, one can identify whether the check node is a zero-ton, singleton or multi-ton with overwhelmingly high reliability. We will therefore assume henceforth that by processing the observations at each check node, we can reliably identify if it is a zero-ton, a singleton or a multi-ton. Additionally if a check node is a singleton, then we know the value as well as the location of the corresponding DFT coefficient.

The FFAST decoder then repeats the following steps (also see pseudocode in Algorithm 1):

- 1) Select all the edges in the graph with right degree 1 (edges connected to singletons).
- 2) Remove these edges from the graph as well as the associated left and right nodes.
- 3) Remove all the other edges that were connected to the left nodes removed in step-2. When a neighboring edge of any right node is removed, its contribution is subtracted from that check node.

Decoding is successful if, at the end, all the edges have been removed from the graph. It is easy to verify that performing the peeling procedure on the example graph of Fig. 6 results in successful decoding, with the coefficients being uncovered in the following possible order: $X_{10}, X_3, X_1, X_5, X_{13}$.

One can also think of the FFAST decoder as a message-passing algorithm. The check nodes pass a message⁹ saying either “no-information” (in the case of a zero-ton or multi-ton), or the value and identity of the variable node (in the case of a singleton). The variable nodes in turn just forward this message to the other check nodes. One round of messages passed back and forth between variable nodes and check nodes is called an *iteration* of the decoder.

We have illustrated how computing a sparse DFT can be translated into a decoding problem over sparse-graphs. Clearly the success of this fast decoder will depend on the properties of the resulting graph. How to get “good” graphs that will result in a low complexity as well as a fast and reliable decoding will be addressed in the next section.

V. PERFORMANCE ANALYSIS OF THE FFAST ALGORITHM FOR THE *very-sparse* ($k \propto n^\delta$, $0 < \delta \leq 1/3$) REGIME

In the previous section, we showed that the problem of computing a k -sparse n -point DFT of a signal can be transformed into a problem of decoding over sparse bipartite graphs using the FFAST architecture. In this section, we describe how to choose a set of uniform sub-sampling patterns, guided by the CRT, to induce a good sparse-graph code. As shown in Section IV-B, the FFAST decoding process is closely related to the decoding procedure on sparse-graph codes designed for erasure channels. From the coding theory literature, we know that there exist several sparse-graph code constructions that are low-complexity and capacity-achieving for the erasure channels. The catch for us is that we are not at liberty to use any arbitrary bi-partite graph, but *can choose only those graphs that can be induced through our proposed subsampling*. Next, we show that a *deterministic* bi-partite graph construction based on the Chinese-Remainder-Theorem (CRT), in conjunction with a *uniformly random* support of the non-zero DFT coefficients, creates sparse-graph codes that: a) have all the good properties that are sufficient for reliable decoding; and b) can be induced using the FFAST subsampling architecture.

We describe two ensembles of bi-partite graphs, the first based on a “balls-and-bins” model, and the second using a deterministic construction based on the CRT. Later, in Lemma 4, we show that the two ensembles are equivalent.

Let $\mathcal{F} = \{f_0, \dots, f_{d-1}\}$, be a set of pairwise co-prime integers and $m \triangleq \sum_{i=0}^{d-1} f_i$. As explained in Table I, the integers f_i ’s are the number of samples per sub-stream in the d stages of the FFAST architecture (see Fig. 2). The integers f_i ’s are approximately equal and we use \mathbf{F} to denote this value.

⁸For the case when the signal has an approximately sparse DFT, more observations per check node will be needed to robustly identify whether the check node is a zero-ton, singleton or multi-ton. I.e., in Fig. 2, D will no longer be 2 as in the exactly sparse case.

⁹In this paper we focus on a low-complexity message passing algorithm where the messages from the check nodes to the variable nodes are hard-decision: either “singleton” or “no-information”. One can implement “softer” and more complex variants of this message-passing algorithm, especially when dealing with the noisy case.

Algorithm 1 FFAST Algorithm

1: *Inputs:*

- A discrete time signal \mathbf{x} of length n , whose n -point DFT \mathbf{X} has at most k non-zero coefficients, where $k \propto n^\delta$.
 - The subsampling parameters of the FFAST architecture (see Fig. 2):
 - the number of stages d .
 - the number of samples per sub-stream in each of the d stages $\mathcal{F} = \{f_0, f_1, \dots, f_{d-1}\}$.are chosen as discussed in Sections V and VI.
-

2: *Output:* An estimate of the k -sparse n -point DFT $\hat{\mathbf{X}}$.

3: *Subsampling:* The input signal \mathbf{x} and its unit delayed version, are uniformly subsampled by $\{n/f_i\}_{i=0}^{d-1}$, to get $D = 2$ sub-streams of the sampled input data per stage (see Fig. 2). The total number of samples $M = 2 \sum_{i=0}^{d-1} f_i$.

4: *Compute short DFTs:*

- Compute an f_i -length DFT of each of the 2 sub-streams in the d stages for $i = 0, 1, \dots, d-1$.
 - This results in a bi-partite graph, with k variable nodes on the left and $m = \sum_{i=0}^{d-1} f_i$ check nodes on the right, where each check node has two observations (see Fig. 6 for an example).
-

5: *FFAST Decoding:* Set the initial estimate of the n -point DFT $\hat{\mathbf{X}} = 0$. Let ℓ denote the number of iterations performed by the FFAST decoder.

6: **for** each iteration **do**

7: **for** each check node **do**

8: Let $(y[0], y[1])$ be the two observations of the check node.

9: **if** $y[0] = y[1] = 0$ **then**

10: the check node is a *zero-ton*.

11: **else**

12: *singleton-test:* If the location estimate $\hat{loc} = \frac{n}{2\pi} (\angle y[1] - \angle y[0])$, is an integer between 0 and $n-1$, then the check node is a *singleton*.

13: *Peeling:* If the check node is a singleton set $\hat{\mathbf{X}}[\hat{loc}] = y[0]$. Subtract the contribution of (peel-off) $\hat{\mathbf{X}}[\hat{loc}]$ from all the neighboring check nodes.

14: **else**

15: the check node is a *multi-ton*.

16: **end if**

17: **end for**

18: **end for**

More precisely, $f_i = \mathbf{F} + O(1)$ for $i = 0, \dots, d-1$, where \mathbf{F} is an asymptotically large number. The $O(1)$ perturbation term in each f_i is used to obtain a set of co-prime integers near \mathbf{F} . Note, that the total number of samples used by the FFAST algorithm is $M = 2d\mathbf{F} + O(1)$ (see Fig. 2). In this section, we use $\mathbf{F} = \eta k$, for some constant η , which results in an order optimal sample complexity $M = O(k)$, but the constructions and results trivially extend to the case when $M > O(k)$.

A. Randomized construction based on the “Balls-and-Bins” model: $\mathcal{C}_1^k(\mathcal{F}, m)$

We construct a bi-partite graph with k variable nodes on the left and m check nodes on the right. The bipartite graphs that we consider in this paper have each variable node v connected to exactly d check nodes, while the edge degree of the check nodes is variable, i.e., left-regular degree bi-partite graphs. An example graph from an ensemble $\mathcal{C}_1^k(\mathcal{F}, m)$, for $\mathcal{F} = \{4, 5\}$, $d = 2$, $k = 5$ and $m = 9$ is provided in Fig. 6. More generally, the ensemble $\mathcal{C}_1^k(\mathcal{F}, m)$ of d -left regular degree bipartite graphs constructed using a “balls-and-bins” model is defined as follows. Partition the set of m check nodes into d subsets with the i^{th} subset having f_i check nodes. For each variable node, choose one neighboring check node in each of the d subsets, uniformly at random. The corresponding d -left regular degree bipartite graph is then defined by connecting the variable nodes with their neighboring check nodes by an undirected edge.

An edge e in the graph is represented as a pair of nodes $e = \{v, c\}$, where v and c are the variable and check nodes incident on the edge e . By a directed edge \vec{e} we mean an ordered pair (v, c) or (c, v) corresponding to the edge $e = \{v, c\}$. A path in the graph is a directed sequence of directed edges $\vec{e}_1, \dots, \vec{e}_t$ such that, if $\vec{e}_i = (u_i, u'_i)$, then the $u'_i = u_{i+1}$ for $i = 1, \dots, t-1$. The length of the path is the number of directed edges in it, and we say that the path connecting u_1 to u_t starts from u_1 and ends at u_t .

1) *Directed Neighborhood*: The directed neighborhood of depth ℓ of $\vec{e} = (v, c)$, denoted by $\mathcal{N}_{\vec{e}}^\ell$, is defined as the induced subgraph containing all the edges and nodes on paths $\vec{e}_1, \dots, \vec{e}_\ell$ starting at node v such that $\vec{e}_1 \neq \vec{e}$. An example of a directed neighborhood of depth $\ell = 2$ is given in Fig. 8. If the induced sub-graph corresponding to the directed neighborhood $\mathcal{N}_{\vec{e}}^\ell$ is a tree then we say that the neighborhood of the edge \vec{e} is *tree-like*.

B. Ensemble of bipartite graphs constructed using the Chinese-Remainder-Theorem (CRT): $\mathcal{C}_2^k(\mathcal{F}, n)$

Let $n \triangleq \prod_{i=0}^{d-1} f_i$. The ensemble $\mathcal{C}_2^k(\mathcal{F}, n)$ of d -left regular degree bipartite graphs, with k variable nodes and m check nodes, is defined as follows. Partition the set of m check nodes into d subsets with the i^{th} subset having f_i check nodes (see Fig. 6 for an example). Consider a set \mathcal{I} of k integers, where each element of the set \mathcal{I} is chosen uniformly at random, with replacement, between 0 and $n-1$. Assign the k integers from the set \mathcal{I} to the k variable nodes in an arbitrary order. Label the check nodes in the set i from 0 to $f_i - 1$ for all $i = 0, \dots, d-1$. A d -left regular degree bi-partite graph with k variable nodes and m check nodes, is then obtained by connecting a variable node with an associated integer v to a check node $(v)_{f_i}$ in the set i , for $i = 0, \dots, d-1$. The ensemble $\mathcal{C}_2^k(\mathcal{F}, n)$ is a collection of all the d -left regular degree bipartite graphs induced by all possible sets \mathcal{I} . A uniformly random choice of integers in the set \mathcal{I} , implies that all the graphs in the ensemble $\mathcal{C}_2^k(\mathcal{F}, n)$ occur with equal probability.

Note that the modulo rule used to generate a graph in the ensemble $\mathcal{C}_2^k(\mathcal{F}, n)$ is same as the one used in equation (4) of Section IV. Thus, the FFAST architecture of Fig. 4 described in Section IV, generates graphs from the CRT ensemble $\mathcal{C}_2^k(\mathcal{F}, n)$, where the indices \mathcal{I} of the k variable nodes are the locations of the non-zero DFT coefficients¹⁰ of the signal \mathbf{x} .

Lemma 4. The ensemble of bipartite graphs $\mathcal{C}_1^k(\mathcal{F}, m)$ is identical to the ensemble $\mathcal{C}_2^k(\mathcal{F}, n)$.

Proof: It is trivial to see that $\mathcal{C}_2^k(\mathcal{F}, n) \subset \mathcal{C}_1^k(\mathcal{F}, m)$. Next we show the reverse. Consider a graph $\mathcal{G}_1 \in \mathcal{C}_1^k(\mathcal{F}, m)$. Suppose, a variable node $v \in \mathcal{G}_1$ is connected to the check nodes $\{a_i\}_{i=0}^{d-1}$. Then, using the CRT, one can find a unique integer q between 0 and $n-1$ such that $(q)_{f_i} = a_i \forall i = 0, \dots, d-1$. Thus, for every graph $\mathcal{G}_1 \in \mathcal{C}_1^k(\mathcal{F}, m)$, there exists a set \mathcal{I} of k integers, that will result in an identical graph using the CRT based construction. Hence, $\mathcal{C}_1^k(\mathcal{F}, m) = \mathcal{C}_2^k(\mathcal{F}, n)$. ■

¹⁰The integers in the set \mathcal{I} are chosen uniformly at random, with replacement, between 0 and $n-1$. A set \mathcal{I} with repeated elements then corresponds to a signal with fewer than k non-zero DFT coefficients.

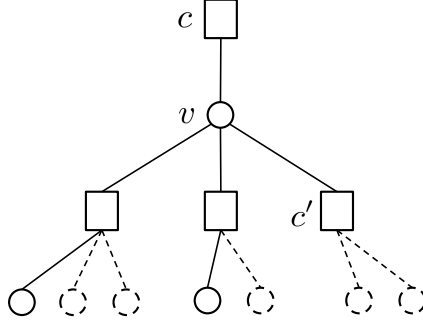


Fig. 8: Directed neighborhood of depth 2 of an edge $\vec{e} = (v, c)$. The dashed lines correspond to nodes/edges removed at the end of iteration j . The edge between v and c can be potentially removed at iteration $j + 1$ as one of the check nodes c' is a singleton (it has no more variable nodes remaining at the end of iteration j).

Next, we analyze the performance of the peeling-decoder over a random choice of a graph from the ensemble $\mathcal{C}_1^k(\mathcal{F}, m)$, which, using the Lemma 4, along with the fact that all the graphs in both the ensembles occur with equal probability, provides a lower bound on the probability of successful decoding of the FFAST decoder over graphs in the ensemble $\mathcal{C}_2^k(\mathcal{F}, n)$.

C. Performance analysis of the peeling-decoder on graphs from the ensemble $\mathcal{C}_1^k(\mathcal{F}, m)$

In this section we analyze the probability of success of the peeling-decoder, over a randomly chosen graph from the ensemble $\mathcal{C}_1^k(\mathcal{F}, m)$, after a fixed number of iterations ℓ . Our analysis follows exactly the arguments in [31] and [32]. Thus, one may be tempted to take the results from [31] “off-the-shelf”. However, we choose here to provide a detailed analysis for two reasons. First, our graph construction in the ensemble $\mathcal{C}_1^k(\mathcal{F}, m)$ is different from that used in [31], which results in some fairly important differences in the analysis, such as the expansion properties of the graphs, thus warranting an independent analysis. Secondly we want to make the paper more self-contained and complete.

We now provide a brief outline of the proof elements highlighting the main technical components needed to show that the peeling-decoder decodes all the non-zero DFT coefficients with high probability.

- *Density evolution:* We analyze the performance of the message-passing algorithm, over a typical graph from the ensemble, for ℓ iterations. First, we assume that a local neighborhood of depth 2ℓ of every edge in a typical graph in the ensemble is tree-like, i.e., cycle-free. Under this assumption, all the messages between variable nodes and the check nodes, in the first ℓ rounds of the algorithm, are independent. Using this independence assumption, we derive a recursive equation that represents the expected evolution of the number of singletons uncovered at each round for this typical graph.
- *Convergence to the cycle-free, case:* Using a Doob martingale as in [31], we show that a random graph from the ensemble, chosen as per nature’s choice of the non-zero DFT coefficients, behaves like a “typical” graph, i.e., 2ℓ -depth neighborhood of most of the edges in the graph is cycle-free, with high probability. This proves that for a random graph in $\mathcal{C}_1^k(\mathcal{F}, m)$, the peeling-decoder decodes all but an arbitrarily small fraction of the variable nodes with high probability in a constant number of iterations, ℓ .
- *Completing the decoding using the graph expansion property:* We first show that if a graph is an “expander” (as will be defined later in Section V-C3), and the peeling-decoder successfully decodes all but a small fraction of the non-zero DFT coefficients, then it decodes all the non-zero DFT coefficients successfully. Next, we show that a random graph from the ensemble $\mathcal{C}_1^k(\mathcal{F}, m)$ is an expander with high probability.

1) **Density evolution for local tree-like view:** In this section we assume that a local neighborhood of depth 2ℓ of every edge in a graph in the ensemble is tree-like. Next, we define the edge-degree distribution polynomials of the bipartite graphs in the ensemble as $\lambda(\alpha) \triangleq \sum_{i=1}^{\infty} \lambda_i \alpha^{i-1}$ and $\rho(\alpha) \triangleq \sum_{i=1}^{\infty} \rho_i \alpha^{i-1}$, where λ_i (resp. ρ_i) denotes the probability that an edge of the graph is connected to a left (resp. right) node of degree i . Thus for the ensemble $\mathcal{C}_1^k(\mathcal{F}, m)$, constructed using the balls-and-bins procedure, $\lambda(\alpha) = \alpha^{d-1}$ by construction. Further, as shown in Appendix A, the edge degree distribution $\rho(\alpha) = \exp(-(1-\alpha)/\eta)$.

Let p_j denote the probability that an edge is present after round j of the peeling-decoder, then $p_0 = 1$. Under the tree-like assumption, the probability p_{j+1} , is given as,

$$p_{j+1} = \lambda(1 - \rho(1 - p_j)) \quad j = 0, 1, \dots, \ell - 1. \quad (5)$$

Equation (5) can be understood as follows (also see Fig. 8): the tree-like assumption implies that, up to iteration ℓ , messages on different edges are independent. Thus, the total probability, that at iteration $j+1$, a variable node v is *decoded* due to a particular check node is given by $\rho(1 - p_j) = \sum_{i=1}^{\infty} \rho_i (1 - p_j)^{i-1}$ and similarly the total probability that none of the neighboring check nodes decode the variable node v is $p_{j+1} = \lambda(1 - \rho(1 - p_j))$. Specializing equation (5) for the edge degree distributions of $\mathcal{C}_1^k(\mathcal{F}, m)$ we get,

$$p_{j+1} = \left(1 - e^{-\frac{p_j}{\eta}}\right)^{d-1}, \quad \forall j = 0, 1, \dots, \ell - 1 \quad (6)$$

where $p_0 = 1$. The evolution process of (6) asymptotically (in the number of iterations ℓ) converges to 0 for appropriate choice of the parameter η , e.g., see Table IV.

d	2	3	4	5	6	7	8	9
η	1.0000	0.4073	0.3237	0.2850	0.2616	0.2456	0.2336	0.2244
$d\eta$	2.0000	1.2219	1.2948	1.4250	1.5696	1.7192	1.8688	2.0196

TABLE IV: Minimum value of η , the average number of bins or check nodes per stage per variable node, required for the density evolution of (6) to converge asymptotically. The threshold value of η depends on the number of stages d . Although, the minimum threshold of η decreases with increasing d , the total number ($\approx d\eta k$) of bins or check nodes required for the convergence of (6) is a not a monotonic function in d .

2) **Convergence to cycle-free case:** In Lemma 5 we show that: a) the expected behavior over all the graphs in the ensemble $\mathcal{C}_1^k(\mathcal{F}, m)$ converges to that of a cycle-free case, and b) with exponentially high probability, almost all the edges in a random graph in the ensemble have a tree-like neighborhood, while the proportion of the edges that are not decoded after ℓ iterations of the peeling-decoder is tightly concentrated around p_ℓ , as defined in (6).

Lemma 5 (Convergence to Cycle-free case). *Over the probability space of all graphs $\mathcal{C}_1^k(\mathcal{F}, m)$, let Z be the total number of edges that are not decoded after ℓ (an arbitrarily large but fixed) iterations of the peeling-decoder over a randomly chosen graph. Further let p_ℓ be as given in the recursion (6). Then there exist constants β and γ such that for any $\epsilon_1 > 0$ and sufficiently large k we have*

$$(a) \quad \mathbb{E}[Z] < kdp_\ell + \frac{d\gamma}{\eta}; \quad (7)$$

$$(b) \quad \Pr(|Z - kdp_\ell| > k\epsilon) < 2e^{-\beta\epsilon_1^2 k}, \quad (8)$$

where $\gamma > 0$ is a constant.

Proof: Please see Appendix D. ■

3) **Successful Decoding using Expansion:** In the previous section we showed that with high probability, i.e., with probability approaching 1 exponentially in k , the peeling-decoder decodes all but an arbitrarily small fraction of variable nodes. In this section, we show how to complete the decoding if the graph is a “good-expander”. Our problem requires the following definition of an “expander-graph”, which is somewhat different from conventional notions of an expander-graph in literature, e.g., *edge expander*, *vertex expander* or *spectral expander* graphs.

Definition 6 (Expander graph). A d -left regular degree bipartite graph constructed as described in Section V-A is called an (α, β, d) expander, if for all subsets S , of variable nodes, of size at most αk , there exists a right neighborhood of S , i.e., $N_i(S)$, that satisfies $|N_i(S)| > \beta|S|$ for some $i = 0, \dots, d-1$.

In the following lemma, we show that if a graph is an expander, and if the peeling-decoder successfully decodes all but a small fraction of the non-zero DFT coefficients, then it decodes all the non-zero DFT coefficients successfully.

Lemma 7. Consider a graph from the ensemble $\mathcal{C}_1^k(\mathcal{F}, m)$, with $|\mathcal{F}| = d$, that is an $(\alpha, 1/2, d)$ expander for some $\alpha > 0$. If the peeling-decoder over this graph succeeds in decoding all but at most αk variable nodes, then it decodes all the variable nodes.

Proof: See Appendix B ■

In Lemma 8, we show that most of the graphs in the ensemble $\mathcal{C}_1^k(\mathcal{F}, m)$ are expanders.

Lemma 8. Consider a random graph from the ensemble $\mathcal{C}_1^k(\mathcal{F}, m)$, where $d \geq 3$. Then, all the subsets S of the variable nodes, of the graph, satisfy $\max_{i=0}^{d-1} |N_i(S)| > |S|/2$,

- a) with probability at least $1 - e^{-\epsilon k \log(m/k)}$, for sets of size $|S| = \alpha k$, for small enough $\alpha > 0$ and some $\epsilon > 0$.
- b) with probability at least $1 - O(1/m)$, for sets of size $|S| = o(k)$.

Proof: See Appendix C ■

The condition $d \geq 3$ is a necessary condition for part (b) of Lemma 8. This can be seen as follows. Consider a random graph from the ensemble $\mathcal{C}_1^k(\mathcal{F}, m)$, where $|\mathcal{F}| = d$. If any two variable nodes in the graph have the same set of d neighboring check nodes, then the expander condition, for the set S consisting of these two variable nodes, will not be satisfied. In a bi-partite graph from the ensemble $\mathcal{C}_1^k(\mathcal{F}, m)$, there are a total of $O(k^d)$ distinct sets of d check nodes. Each of the k variable nodes chooses a set of d check nodes, uniformly at random and with replacement, from the total of $O(k^d)$ sets. If we draw k integers uniformly at random between 0 to $n - 1$, the probability $Pr(k; n)$ that at least two numbers are the same is given by,

$$Pr(k; n) \approx 1 - e^{-k^2/2n}. \quad (9)$$

This is also known as the *birthday paradox* or the *birthday problem* in literature [33]. For a graph from the ensemble $\mathcal{C}_1^k(\mathcal{F}, m)$, we have $n = O(k^d)$. Hence, if the number of stages $d \leq 2$, there is a constant probability that there exists a pair of variable nodes that share the same neighboring check nodes, in both the stages, thus violating the expander condition.

Theorem 9. The peeling-decoder over a random graph from the ensemble $\mathcal{C}_1^k(\mathcal{F}, m)$, where $d \geq 3$ and $F = \eta k$:

- a) successfully uncovers all the variable nodes with probability at least $1 - O(1/m)$;
 - b) successfully uncovers all but a vanishingly small fraction, i.e., $o(k)$, of the variable nodes with probability at least $1 - e^{-\epsilon k \log(m/k)}$, for some $\epsilon > 0$,
- for an appropriate choice of the constant η as per Table IV.

Proof: Let Z be the number of edges not decoded by the peeling-decoder in ℓ (large but fixed constant) iterations. Then, from recursion (6) and Lemma 5, for an appropriate choice of the constant η (as per Table IV), $Z \leq \alpha k$, for an arbitrarily small constant $\alpha > 0$, with probability at least $1 - e^{-\beta \epsilon_1^2 k}$. The result then follows from Lemmas 8 and 7. \blacksquare

D. Performance of the FFAST-decoder over graphs in $\mathcal{C}_2^k\{\mathcal{F}, n\}$ for $k \propto n^\delta$, for $(0 < \delta \leq 1/3)$.

In earlier sections, we discussed at length a simple iterative peeling-like decoding over random graphs constructed using a balls-and-bins model as described in Section V-A. In this section we connect this discussion to the problem of computing a k -sparse n -point DFT of a signal, where $k \propto n^\delta$, and $(0 < \delta \leq 1/3)$.

Consider a $d = 3$ stage FFAST architecture, i.e., $\mathcal{F} = \{f_0, f_1, f_2\}$. Let $\mathbf{F} = \eta k$, where η is an appropriately chosen constant (see Table IV in Section V-C1), $n_1 = \prod_{i=0}^2 f_i$ and $n = n_1 \mathcal{P}$ for some integer $\mathcal{P} \geq 1$, i.e., $k \propto n^\delta$, and $0 < \delta \leq 1/3$. As \mathcal{P} increases, δ approaches 0.

For $\mathcal{P} = 1$, the CRT guarantees that every integer j between 0 and $n - 1$ is uniquely represented by a triplet $((j)_{f_0}, (j)_{f_1}, (j)_{f_2})$. However for $\mathcal{P} > 1$, such a statement does not hold. For example, when $\mathcal{P} = 2$, for every triplet (r_0, r_1, r_2) there are exactly two numbers between 0 and $n - 1$ that have (r_0, r_1, r_2) as remainders modulo $f_i, i = 0, 1, 2$. Hence, the only difference between $\mathcal{P} = 1$ and $\mathcal{P} > 1$ in terms of the resulting bi-partite graph is whether or not multiple variable nodes (the non-zero DFT coefficients) have identical neighboring check nodes in all the 3 stages. Recall, in the balls-and-bins ensemble $\mathcal{C}_1^k(\mathcal{F}, m)$ described in Section V-A, we did allow for multiple variable nodes to share an identical set of check nodes. Despite this, we showed in Theorem 9 that the peeling-decoder successfully decodes the values of all the variable nodes with high probability. As a result, the proof of Theorem 2 for the *very-sparse* regime then follows from Lemma 4 and Theorem 9. \square

VI. PERFORMANCE ANALYSIS OF THE FFAST ALGORITHM FOR THE *less-sparse* ($k \propto n^\delta$, $1/3 < \delta < 1$) REGIME

In the previous section, we analyzed the performance of the FFAST algorithm for the very-sparse regime ($k \propto n^\delta$, $0 < \delta \leq 1/3$). Recall that for the very-sparse regime, the integers in the set $\mathcal{F} = \{f_0, \dots, f_{d-1}\}$, i.e., the number of samples per sub-stream in the d different stages, are pairwise co-prime. For the less-sparse regime ($k \propto n^\delta$, $1/3 < \delta < 1$) the relation between the integers f_i 's is bit more involved. So, for ease of exposition in this section, we describe the achievable FFAST construction for a special case of $k \propto n^{2/3}$, i.e., $\delta = 2/3$, which generalizes to the regimes $\delta = 1 - 1/d$, for integer values of $d \geq 3$, through an induction argument. Later in Section VI-C we show how to achieve the intermediate values of δ . To summarize, our approach for the less-sparse regime is as follows.

- First we analyze the performance of the FFAST algorithm for $\delta = 2/3$. Then, in Section VI-B, we provide a brief sketch of how to generalize the FFAST architecture to any $\delta = 1 - 1/d$, for integer values of $d \geq 3$. This covers the range of values of $\delta = 2/3, 3/4, \dots$
- In Section VI-C, we show how to achieve the intermediate values of δ , thus covering the entire range of the sparsity index $1/3 < \delta < 1$.

A. Less-sparse regime of $\delta = 2/3$

Let $\{\mathcal{P}_0, \mathcal{P}_1, \mathcal{P}_2\}$, be a set of pairwise co-prime integers such that $\mathcal{P}_i = \mathbf{F} + O(1)$, $i = 0, 1, 2$, for some large integer \mathbf{F} . Set $k \propto \mathbf{F}^2$ and $n = \prod_{i=0}^2 \mathcal{P}_i$, i.e., $k \propto n^{2/3}$. Also, let $f_0 = \mathcal{P}_0 \mathcal{P}_1$, $f_1 = \mathcal{P}_1 \mathcal{P}_2$ and $f_2 = \mathcal{P}_2 \mathcal{P}_3$.

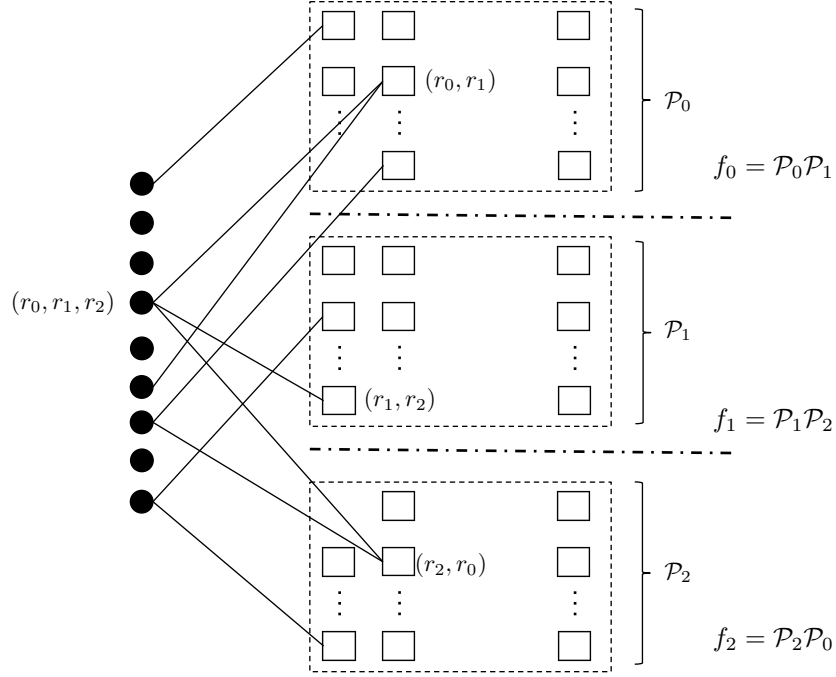


Fig. 9: A bi-partite graph with k variable nodes and $m = \sum_{i=0}^2 f_i$ check nodes, constructed using a balls-and-bins model. The check nodes in each of the 3 sets are arranged in a matrix format, e.g., the f_0 check nodes in the set 0 are arranged in \mathcal{P}_0 rows and \mathcal{P}_1 columns. A check node in row r_0 and column r_1 in the set 0, is indexed by a pair (r_0, r_1) and so on and so forth for all the other check nodes. Each variable node chooses a triplet (r_0, r_1, r_2) , where r_i is between 0 and $\mathcal{P}_i - 1$ uniformly at random. A 3-regular degree bi-partite graph is then constructed by connecting a variable node with a triplet (r_0, r_1, r_2) to the check nodes (r_0, r_1) , (r_1, r_2) and (r_2, r_0) in the three sets of the check nodes respectively.

1) Balls-and-Bins construction: We construct a bi-partite graph with k variable nodes on the left and $m = \sum_{i=0}^2 f_i$, check nodes on the right (see Fig. 9) using balls-and-bins model as follows. Partition the m check nodes into 3 sets/stages containing f_0 , f_1 and f_2 check nodes respectively. The check nodes in each of the 3 sets are arranged in a matrix format as shown in Fig. 9, e.g., f_0 check nodes in the set 0 are arranged in \mathcal{P}_0 rows and \mathcal{P}_1 columns. A check node in row r_0 and column r_1 in the set 0, is indexed by a pair (r_0, r_1) and so on and so forth for all the other check nodes. Each variable node chooses a triplet (r_0, r_1, r_2) , where r_i is between 0 and $\mathcal{P}_i - 1$ uniformly at random. The triplets are chosen with replacement and independently across all k variable nodes. A 3-regular degree bi-partite graph with k variable nodes and m check nodes is then constructed by connecting a variable node with a triplet (r_0, r_1, r_2) to the check nodes (r_0, r_1) , (r_1, r_2) and (r_2, r_0) in the three sets of check nodes respectively, e.g., see Fig. 9.

2) Connection to the CRT based bi-partite graphs induced by the FFAST architecture: Each variable node is associated with an integer v between 0 and $n - 1$ (location of the DFT coefficient). As a result of the subsampling and computing a smaller DFTs in the FFAST architecture (see Fig 2), a variable node with an index v is connected to the check nodes $(v)_{f_0}$, $(v)_{f_1}$ and $(v)_{f_2}$ in the 3 stages, in the resulting aliased bi-partite graph. The CRT implies that v is uniquely represented by a triplet (r_0, r_1, r_2) , where $r_i = (v)_{\mathcal{P}_i}$. Also, $((v)_{f_i})_{\mathcal{P}_i} = (v)_{\mathcal{P}_i} = r_i$, for all $i = 0, 1, 2$. Thus, the FFAST architecture induces a 3-regular degree bi-partite graph with k variable nodes and m check nodes, where a variable node with an associated triplet (r_0, r_1, r_2) is connected to the check nodes (r_0, r_1) , (r_1, r_2) and (r_2, r_0) in the three sets respectively. Further, a uniformly random model for the support v of a non-zero DFT coefficient, corresponds to choosing the triplet (r_0, r_1, r_2) uniformly at random. Thus, the CRT based construction, induced by the FFAST architecture, is equivalent to the balls-and-bins construction discussed in the Section VI-A1.

Following the outline of the proof of Theorem 2 (provided in Section V), one can show the following, for the balls-and-bins construction of Section VI-A1:

- 1) *Density evolution for the cycle-free case*: Assuming a local tree-like neighborhood derive a recursive equation (similar to equation 6) representing the expected evolution of the number of singletons uncovered at each round for a “typical” graph from the ensemble.
- 2) *Convergence to the cycle-free case*: Using a Doob martingale show an equivalent of Lemma 5 for the less-sparse regime, where the number of check nodes in the 3 different stages f_0 , f_1 and f_2 are not pairwise co-prime.
- 3) *Completing the decoding using the graph expansion property*: A random graph from the ensemble is a good expander with high probability. Hence, if the FFAST decoder successfully decodes all but a constant fraction of variable nodes, it decodes all the variable nodes.

The analysis of the first two items for the less-sparse regime is similar in spirit to the one in Section V, and will be skipped here. However, the analysis of the third item will be described here as there are some key differences, mainly arising from the nature of the overlapping co-prime number of check nodes in the bi-partite graphs for the less-sparse regime in contrast to the very-sparse regime. In Section V, for the very-sparse regime we showed (in Lemma 8) that the bottleneck failure event is not being able to decode *all* the DFT coefficients. In this section, we analyze this bottleneck failure event for the case of the less-sparse regime. In particular, we show that if the FFAST decoder has successfully decoded all but a small constant number of DFT coefficients, then it decodes all the DFT coefficients successfully with high probability.

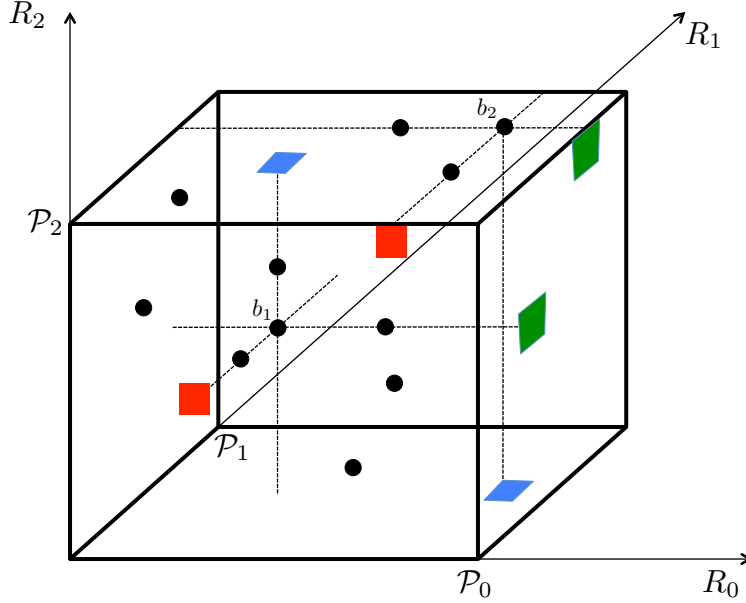


Fig. 10: A 3D visualization of a bipartite graph from the ensemble $\mathcal{C}_2^k(\mathcal{F}, n)$ corresponding to the less-sparse regime of $\delta = 2/3$. Recall that for $\delta = 2/3$, $\{\mathcal{P}_j\}_{j=0}^2$ are pairwise co-prime integers, such that $\mathcal{P}_i \approx \mathbf{F}$, $i = 0, 1, 2$, where \mathbf{F} is a large integer. The set $\mathcal{F} = \{f_0, f_1, f_2\}$, where $f_0 = \mathcal{P}_0\mathcal{P}_1$, $f_1 = \mathcal{P}_1\mathcal{P}_2$ and $f_2 = \mathcal{P}_2\mathcal{P}_0$. The parameters $k \propto \mathbf{F}^2$ and $n = \prod_{i=0}^2 \mathcal{P}_i$, i.e., $k \propto n^{2/3}$. A variable node with an associated triplet (r_0, r_1, r_2) is represented by a ‘ball’ at the position (r_0, r_1, r_2) . The f_0 check nodes in the stage-1 of the bi-partite graph are represented by ‘blue’ squares and likewise the ones in f_1 are ‘green’ and the check nodes in stage f_2 are ‘red’. All the neighboring check nodes of a variable node, e.g., b_1 , are multi-ton iff there is at least one more variable node along each of the three directions R_0, R_1 and R_2 . The green and red neighboring check nodes connected to the ball b_2 are multi-tons, while the blue neighboring check node is a singleton since there are no other variable nodes along the R_2 direction of b_2 .

3) Decoding all the variable nodes using the expansion properties of the CRT construction:

Consider an alternative visualization of a random bi-partite graph from the ensemble $\mathcal{C}_2^k(\mathcal{F}, n)$ as shown in Fig. 10. A variable node associated with a triplet (r_0, r_1, r_2) is represented by a ball at the position (r_0, r_1, r_2) . The plane R_0 - R_1 corresponds to the check nodes in the stage f_0 , in a sense that all the variable nodes that have identical (r_0, r_1) but distinct r_2 are connected to the check node (r_0, r_1) and so on. Similarly the planes R_1 - R_2 and R_2 - R_0 correspond to the check nodes in stages f_1 and f_2 respectively. Thus, a variable node with co-ordinates (r_0, r_1, r_2) is connected to multi-ton check nodes, if and only if there exist variable nodes with co-ordinates (r_0, r_1, r'_2) , (r'_0, r_1, r_2) and (r_0, r'_1, r_2) (see Fig. 10), i.e., one neighbor in each axis. The FFAST decoder stops decoding if all the check nodes are multi-tons. Next, we find an upper bound on the probability of this ‘bad’ event.

Consider a set S of variable nodes such that $|S| = s$, where s is a small constant. Let E_S be an event that all the neighboring check nodes of all the variable nodes in the set S are multi-tons, i.e., the FFAST decoder fails to decode the set S . Also, let E be an event that there exists such a set. We first compute an upper bound on the probability of the event E_S , and then apply a union bound over all $\binom{k}{s}$ sets to get an upper bound on the probability of the event E .

Each variable node in the set S chooses an integer triplet (r_0, r_1, r_2) uniformly at random in a cube of size $\mathcal{P}_0 \times \mathcal{P}_1 \times \mathcal{P}_2$. Let p_{\max} denote the maximum number of distinct values taken by these s variable nodes on any of the R_i axis. The FFAST decoder fails to decode the set S if and only if all the variable nodes have at least one neighbor along each of the 3 directions R_0, R_1, R_2 (see Fig. 10). This implies that $s \geq 4p_{\max}$. Also, $p_{\max} > 1$, i.e., $s \geq 8$, since by the CRT all the variable nodes s (with distinct associated integers) cannot have an identical triplet (r_0, r_1, r_2) . An upper bound on the probability of the event E_S is then obtained as follows:

$$\begin{aligned}
 \Pr(E_S) &< \prod_{i=0}^2 \left(\frac{s}{4\mathcal{P}_i} \right)^s \left(\frac{\mathcal{P}_i}{s/4} \right) \\
 &\approx \left(\frac{s}{4\mathbf{F}} \right)^{3s} \left(\frac{\mathbf{F}}{s/4} \right)^3 \\
 &\stackrel{(a)}{<} \left(\frac{s}{4\mathbf{F}} \right)^{3s} \left(\frac{4\mathbf{F}e}{s} \right)^{3s/4} \\
 &= \left(\frac{se^{1/3}}{4\mathbf{F}} \right)^{9s/4},
 \end{aligned} \tag{10}$$

where in (a) we used $\binom{p}{q} \leq (p^q/q!) \leq (pe/q)^q$. Then, using a union bound over all possible $\binom{k}{s}$ sets, we get:

$$\begin{aligned}
 \Pr(E) &< \Pr(E_S) \binom{k}{s} \\
 &< \left(\frac{se^{1/3}}{4\mathbf{F}} \right)^{9s/4} \left(\frac{ke}{s} \right)^s \\
 &= O(1/m),
 \end{aligned} \tag{11}$$

where in the last inequality, we used $s \geq 8$, $k \propto \mathbf{F}^2$ and $m = O(\mathbf{F}^2)$.

Thus, the FFAST decoder decodes all the variable nodes with probability at least $1 - O(1/m)$.

B. Sketch of proof for $\delta = 1 - 1/d$, where $d \geq 3$ is an integer

Consider a d -stage FFAST architecture with the following parameters. Let $\{\mathcal{P}_i\}_{i=0}^{d-1}$, be a set of pairwise co-prime integers such that $\mathcal{P}_i = \mathbf{F} + O(1)$, $i = 0, 1, \dots, d-1$, for some large integer \mathbf{F} . Set

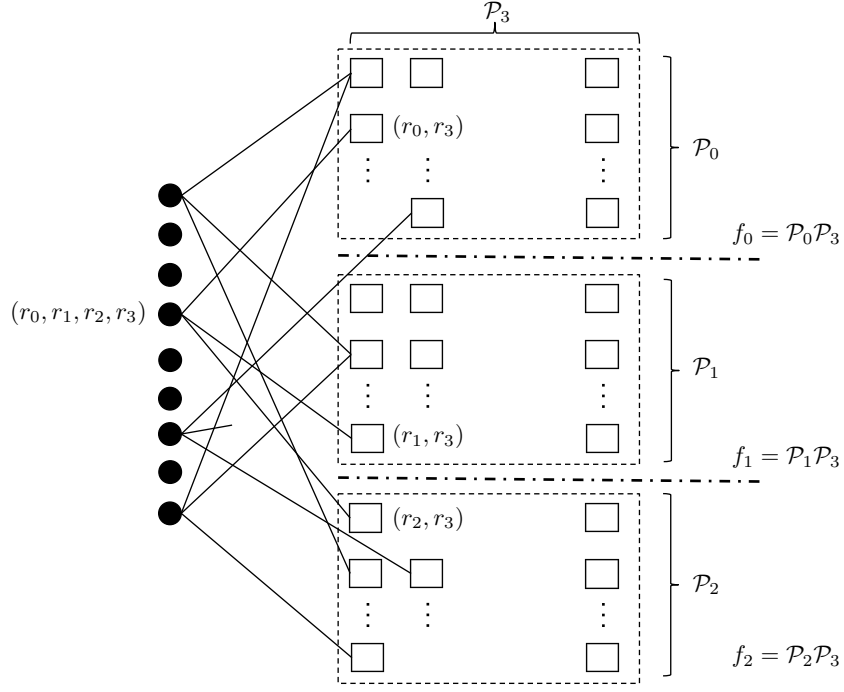


Fig. 11: Let $\{\mathcal{P}_i\}_{i=0}^3$ be a set of pairwise co-prime integers, such that $\mathcal{P}_i \approx \mathbf{F}$, $i = 0, 1, 2$, and $\mathcal{P}_3 \approx \mathbf{F}^a$ for some $a > 0$. Also, let $k \propto \mathbf{F}^{1+a}$, $n = \prod_{i=0}^3 \mathcal{P}_i$ and $f_0 = \mathcal{P}_0 \mathcal{P}_3$, $f_1 = \mathcal{P}_1 \mathcal{P}_3$ and $f_2 = \mathcal{P}_2 \mathcal{P}_3$. The check nodes in each of the 3 sets are arranged so that a j^{th} check node in the set i belongs to the row $(j)_{\mathcal{P}_i}$ and the column $(j)_{\mathcal{P}_3}$. A variable node with an associated integer v is uniquely represented by a quadruplet (r_0, r_1, r_2, r_3) where $r_i = (v)_{\mathcal{P}_i}$, $i = 0, 1, 2, 3$, and is connected to the check node (r_i, r_3) in set i . Thus, the resulting bipartite graph is a union of \mathcal{P}_3 disjoint bi-partite graphs as shown in the figure.

$k \propto \mathbf{F}^{d-1}$ and $n = \prod_{i=0}^{d-1} \mathcal{P}_i$, i.e., $k \propto n^{(d-1)/d}$. Also, let $f_i = \prod_{j=i}^{i+(d-2)} \mathcal{P}_{(j)_d}$, for $i = 0, \dots, d-1$. The expansion property, of this construction for any value of d can be shown as follows:

- Decoding all the variable nodes: For $d = 3$, the worst case event is, the FFAST decoder fails to decode a set of size $|S| = 2^3 = 8$. For a general d , using an induction, one can show that the worst case failure event is when the FFAST decoder fails to decode a set of size $|S| = 2^d$. The probability of this event is upper bounded by $1/\mathbf{F}^{2^d - 2d}$.

C. Achieving the intermediate values of δ

In this section we show how to extend the scheme in Section V, that was designed for $k \propto n^{1/3}$, to achieve a sparsity regime of $k \propto n^{(1+a)/(3+a)}$ for $a > 0$. This extension technique can be essentially used in conjunction with any of the operating points described earlier. Thus covering the full range of sparsity index $0 < \delta < 1$.

Choose a set of integer factors $\{\mathcal{P}_i\}_{i=0}^3$ that are pairwise co-prime and $\mathcal{P}_i = \mathbf{F} + O(1)$, $i = 0, 1, 2$, while $\mathcal{P}_3 = \mathbf{F}^a + O(1)$ for some $a > 0$. Let $k \propto \mathbf{F}^{1+a}$ and $n = \prod_{i=0}^3 \mathcal{P}_i$, i.e., $k \propto n^{(1+a)/(3+a)}$, and $f_0 = \mathcal{P}_0 \mathcal{P}_3$, $f_1 = \mathcal{P}_1 \mathcal{P}_3$ and $f_2 = \mathcal{P}_2 \mathcal{P}_3$.

1) *Union of Disjoint problems:* The check nodes in each of the 3 sets are arranged so that a j^{th} check node in the set i , belongs to the row $(j)_{\mathcal{P}_i}$ and the column $(j)_{\mathcal{P}_3}$ (see Fig. 11). This is always possible using the CRT since $\{\mathcal{P}_i\}_{i=0}^3$ are pairwise co-prime and $f_i = \mathcal{P}_i \mathcal{P}_3$, $i = 0, 1, 2$.

A variable node with an associated integer v is uniquely represented by a quadruplet (r_0, r_1, r_2, r_3) where $r_i = (v)_{\mathcal{P}_i}$, $i = 0, 1, 2, 3$ and is connected to the check node (r_i, r_3) in set i . Thus, the resulting bipartite graph is a union of \mathcal{P}_3 disjoint bi-partite graphs, where each bi-partite subgraph behaves as an instance of the 3-stage perfect co-prime case discussed in Section V. Then, using a union bound over

these disjoint graphs one can compute the probability of the FFAST decoder successfully decoding all but $o(k)$ and all the variable nodes for asymptotic values of k, n .

VII. SAMPLE AND COMPUTATIONAL COMPLEXITY OF THE FFAST ALGORITHM

The FFAST algorithm performs the following operations in order to compute the n point DFT of an n -point discrete-time signal \mathbf{x} (see Algorithm 1 in Section IV)

- 1) **Sub-sampling:** A FFAST architecture (see Fig. 2 in Section I) with d stages, has d distinct subsampling patterns chosen as per the discussions in Sections V and VI. These patterns are deterministic and are pre-computed. We assume the presence of random-access-memory, with unit cost per I/O operation, for reading the subsamples. For the very-sparse regime ($k \propto n^\delta$, $0 < \delta \leq 1/3$) as shown in Section V, the FFAST architecture has $d = 3$ stages and $D = 2$ sub-streams per stage. Hence, the total number of samples used for the very-sparse regime is $M = 2.44k$ (see Section V Table IV). For the less-sparse regime, choice of the FFAST architecture parameters is bit more involved and depends on the sparsity index δ . A $d \leq 8$ stage FFAST architecture, in conjunction with discussion of Section VI-C, is sufficient to achieve the sparsity index of $1/3 < \delta < 0.99$. Thus, again using the values from Table IV of Section V for $d = 8$, for the less-sparse regime of $1/3 < \delta < 0.99$ the number of samples $M \leq 3.74k$. In general for any fixed $0 < \delta < 1$, the sample complexity M can be as small as rk , where r is a constant that depends on the sparsity index δ .
- 2) **DFT:** The FFAST algorithm then computes $2d$ DFT's, each of length approximately equal to k (for an order optimal $M = rk$ sample complexity), of the subsampled input data corresponding to $D = 2$ sub-streams in each of the d stages. Using a standard FFT algorithm, e.g., prime-factor FFT or Winograd FFT algorithm [28], one can compute each of these DFT's in $O(k \log k)$ computations. Thus, the total computational cost of this step is $O(k \log k)$.
- 3) **Peeling-decoder over sparse graph codes:** It is well known [34], that the computational complexity of the peeling-decoder over sparse graph codes is linear in the dimension of the graph, i.e., $O(k)$.

Thus, the FFAST algorithm computes a k -sparse n -point DFT with $O(k)$ samples using no more than $O(k \log k)$ computations for all $0 < \delta < 1$.

VIII. SIMULATION RESULTS

In this section we validate the empirical performance of our FFAST algorithm for a wide variety of 1-D and 2-D DFT settings for signals having an exactly or approximately sparse Fourier spectrum. In Section VIII-A we show the performance of the FFAST algorithm for the 1-D exactly-sparse setting, for two regimes, what we call the *very-sparse* and the *less-sparse* regimes. We contrast the observed empirical performance, in terms of sample complexity, computational complexity and probability of success, with the theoretical claims of Theorem 2. Section VIII-B provides an empirical evidence of the *noise robustness* of the FFAST algorithm for the 1-D setting when the Fourier spectrum of a desired signal is *approximately sparse*. In Section VIII-C, we show, how the 1-D FFAST algorithm described in this paper can be generalized to a 2-D setting and also provide simulation results, of application of the FFAST algorithm, for an exactly and approximately sparse 2-D signals. In the 2-D simulation results provided in Section VIII-C, the amplitude of the non-zero DFT coefficients are complex valued and not limited to the scalar multiples of $\{\pm 1\}$, as is the case for 1-D simulations.

A. Performance of the FFAST algorithm for exactly k -sparse 1-D DFT signals

- **Very sparse regime:** The desired signal \mathbf{x} is of ambient dimension $n = 511 \times 512 \times 513 \approx 134 \times 10^6$. The sparsity parameter k is varied from 400 to 1300 which corresponds to the very-sparse regime of $k \propto n^{1/3}$. We consider a FFAST architecture with $d = 3$ stages and $D = 2$ sub-streams per stage, i.e., two delay chains per stage (see Fig. 2). The uniform sampling periods for the 3 stages

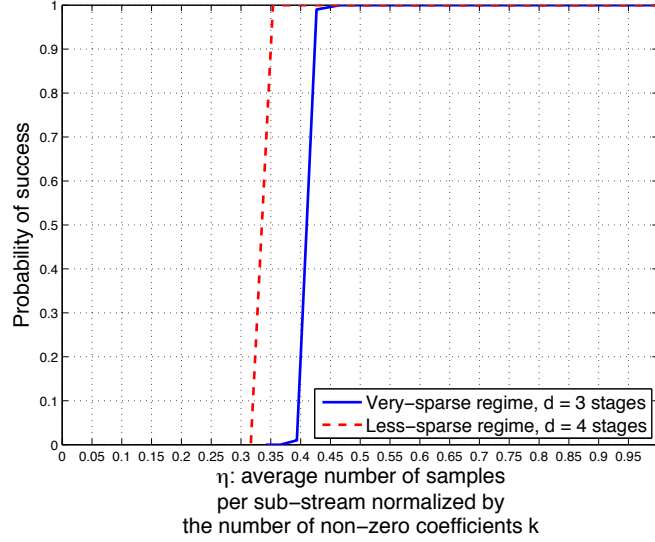


Fig. 12: The probability of success of the FFAST algorithm as a function of η , the average number of samples per sub-stream normalized by the number of non-zero coefficients k . The plot is obtained for the two different sparsity regimes: 1) Very-sparse regime, i.e., $k \propto n^{1/3}$. For this regime, a $d = 3$ stage FFAST architecture is chosen. The number of samples per sub-stream in the three stages are perfectly co-prime, ($f_0 = 511, f_1 = 512$ and $f_2 = 513$), and 2) Less-sparse regime, specifically ($n^{0.73} < k < n^{0.85}$). For this regime, a $d = 4$ stage FFAST architecture is chosen. The number of samples per sub-stream in the 4 stages are not co-prime, ($f_0 = 5168, f_1 = 6783, f_2 = 6384$ and $f_3 = 5712$). Each point on the plot is obtained by averaging over 10000 runs. The ambient signal dimension n and the number of samples M are fixed, while the number of non-zero coefficients k is varied to get different values of η . We note that the FFAST algorithm exhibits a threshold behavior with $\eta_1 = 0.427$ being the threshold for the very-sparse regime, and $\eta_2 = 0.354$ for the less-sparse regime respectively. From Table IV in Section V-C1, we see that the optimal threshold values are $\eta_1^* = 0.4073$ and $\eta_2^* = 0.3237$, which are in close agreement with our simulation results.

are 512×513 , 511×513 and 511×512 respectively. This results in the number of samples per sub-stream, for the three stages to be $f_0 = 511, f_1 = 512$ and $f_2 = 513$ respectively. Note that the number of samples per sub-stream in all the three different stages, i.e., f_i 's, are pairwise co-prime. The total number of samples used by the FFAST algorithm for this simulation is¹¹ $M < 2(f_0 + f_1 + f_2) = 3072$.

- **Less sparse regime:** The desired signal \mathbf{x} is of ambient dimension $n = 16 \times 17 \times 19 \times 21 \approx 0.1 \times 10^6$. The sparsity parameter k is varied from 5000 to 19000 which corresponds to the less-sparse regime of $n^{0.73} < k < n^{0.85}$. We consider a FFAST architecture with $d = 4$ stages and $D = 2$ sub-streams per stage. The uniform sampling periods for the 4 stages are 21, 16, 17 and 19 respectively. This results in the number of samples per sub-stream, for the four stages to be $f_0 = 16 \times 17 \times 19 = 5168, f_1 = 17 \times 19 \times 21 = 6783, f_2 = 19 \times 21 \times 16 = 6384$ and $f_3 = 21 \times 16 \times 17 = 5712$ respectively. Note that the number of samples per sub-stream in the four stages are composed of “cyclically-shifted” co-prime numbers and are not pairwise co-prime. The total number of samples used by the FFAST algorithm for this simulation is $M < 2(f_0 + f_1 + f_2 + f_3) = 48094$.
- For each run, an n -dimensional k -sparse signal \mathbf{X} is generated with non-zero values $X_i \in \{\pm 10\}$ and the positions of the non-zero coefficients are chosen uniformly at random in $\{0, 1, \dots, n-1\}$. The time domain signal \mathbf{x} is then generated from \mathbf{X} using an IDFT operation. This discrete-time

¹¹The samples used by the different sub-streams in the three different stages overlap, e.g., $x[0]$ is common to all the zero delay sub-streams in each stage. Hence, $M < 2(f_0 + f_1 + f_2)$ and not equal.

Sparsity Regimes	Signal dimension n	Sparsity k	$k = n^{\frac{\delta}{\delta}}$	# of stages d	$M \approx 2d\eta k$		ℓ	Number of failures	Runs
					M	η			
Very-sparse	511*512*513 $\approx 134 \times 10^6$	900	0.363	3	3072	0.569	6	1	10000
		1000	0.369		3072	0.512	9	0	10000
		1100	0.374		3072	0.465	13	1	10000
		1200	0.378		3072	0.427	18	99	10000
Less-sparse	16*17*19*21 $\approx 0.1 \times 10^6$	13000	0.81	4	48094	0.462	6	0	10000
		15000	0.83		48094	0.401	8	0	10000
		17000	0.84		48094	0.354	13	2	10000
		19000	0.85		48094	0.316	29	10000	10000

TABLE V: Shows the performance of the FFAST algorithm for two different sparsity regimes: 1) Very-sparse regime: $k \propto n^{1/3}$. For this regime, a $d = 3$ stage FFAST architecture is chosen. The number of samples per sub-stream in each of the 3 stages are perfectly co-prime: $f_0 = 511, f_1 = 512$ and $f_2 = 513$ respectively, and 2) Less-sparse regime: $n^{0.73} < k < n^{0.85}$. For this regime, a $d = 4$ stage FFAST architecture is chosen. The number of samples per sub-stream in each of the 4 stages are *not* co-prime but have “cyclically-shifted” overlapping co-prime factors: $f_0 = 16 \times 17 \times 19 = 5168$, $f_1 = 17 \times 19 \times 21 = 6783$, $f_2 = 19 \times 21 \times 16 = 6384$ and $f_3 = 21 \times 16 \times 17 = 5712$ respectively. We note that the FFAST algorithm exhibits a threshold behavior in terms of sample complexity M . For example, when $\eta_1 \geq 0.427$ and $\eta_2 \geq 0.354$, for the very-sparse and the less-sparse regimes respectively, the FFAST algorithm successfully computes all the non-zero DFT coefficients for almost all the runs. Further, in one or two instances when it failed to recover all the non-zero DFT coefficients, it has recovered all but 8 (for $d = 3$) or 16 (for $d = 4$) non-zero DFT coefficients. This validates our theoretical findings of the bottleneck failure event being that the FFAST decoder decodes all but a handful of the DFT coefficients. From Table IV in Section V-C1, we see that the optimal threshold values for the very-sparse and less-sparse regimes are $\eta_1^* = 0.4073$ and $\eta_2^* = 0.3237$ resp., which are in close agreement with the simulation results. The table also shows that the average number of iterations ℓ , required for the FFAST algorithm to successfully compute the DFT for both the regimes, are quite modest.

signal \mathbf{x} is then given as an input to our FFAST algorithm.

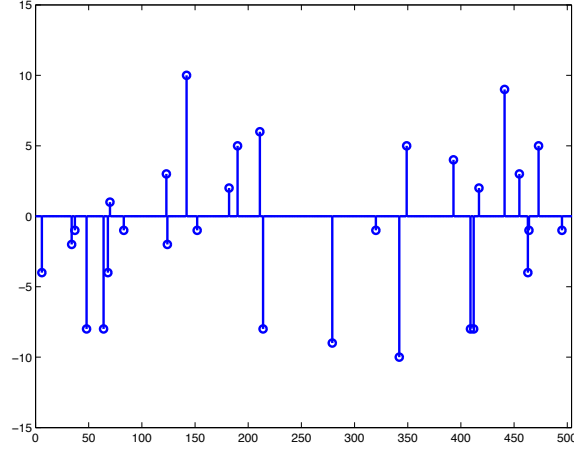
- Each sample point in the Fig. 12, is generated by averaging over 10000 runs.
- Decoding is successful if all the DFT coefficients are recovered perfectly.

We observe the following aspects of the simulations in detail and contrast it with the claims of Theorem 2

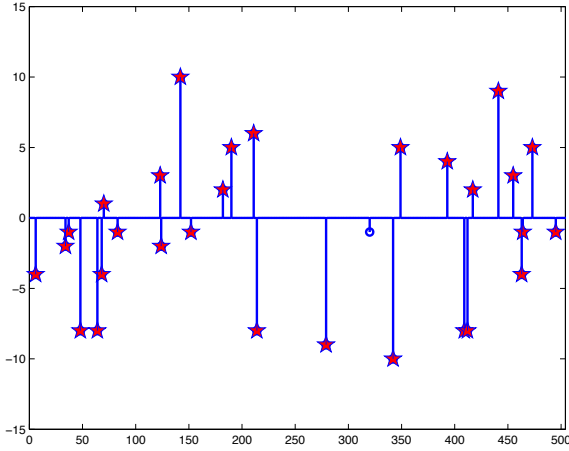
Density Evolution: The density evolution recursion (6) in Section V-C1, implies a threshold behavior: if the average number of samples per sub-stream normalized by k , i.e., η , is above a certain threshold (as specified in Section V-C1 Table IV), then the recursion (6) converges to 0 as $\ell \rightarrow \infty$ otherwise p_ℓ is strictly bounded away from 0. In Fig. 12 we plot the probability of success, averaged over 10000 runs, of the FFAST algorithm as a function of η , i.e., varying k for a fixed number of samples M . We note that the FFAST algorithm exhibits a threshold behavior with $\eta_1 = 0.427$ being the threshold for the very-sparse regime with $d = 3$, and $\eta_2 = 0.354$ for the less-sparse regime with $d = 4$ respectively. From Table IV in Section V-C1, we see that the optimal threshold values are $\eta_1^* = 0.4073$ and $\eta_2^* = 0.3237$, which are in close agreement with our simulation results of Fig. 12.

The FFAST algorithm is verified to compute the DFT with high probability using as few as $M = rk$ samples, where the oversampling ratio $r \approx 2d\eta < 4$ as given in Table IV.

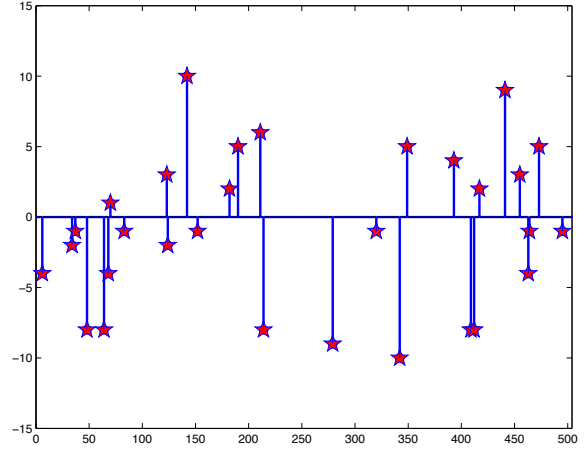
Iterations: In the theoretical analysis of Section V-C2, we showed that the FFAST algorithm, if successful, decodes all the DFT coefficients in ℓ iterations, where, ℓ is a large but a fixed constant. In order to get an empirical sense of how large ℓ has to be, we consider an example with $n = 504$, $k = 30$, and a three-stage FFAST architecture. The number of samples per sub-stream in the three stages are $f_0 = 56, f_1 = 72$ and $f_2 = 63$ respectively. Further, each stage has $D = 2$ delay sub streams. An example of an n -length input signal \mathbf{x} that has a 30-sparse DFT is shown in Fig. 13(a). In this simulation, we observe that the FFAST algorithm computes the sparse DFT \mathbf{X} perfectly in $\ell = 2$ iterations, as shown in Fig 13(c) using $M = 2 \sum_{i=0}^2 f_i = 382$ samples of \mathbf{x} . Note that the number of samples $M > 4k$ for



(a) Original k -sparse n -length DFT \mathbf{X} , where $k = 30$ and $n = 504$.



(b) Estimated signal $\hat{\mathbf{X}}$ after 1 iteration.



(c) Estimated signal $\hat{\mathbf{X}} = \mathbf{X}$ after 2 iterations.

Fig. 13: Consider a FFAST architecture with $d = 3$ stages, ambient signal dimension $n = 504$ and sparsity $k = 30$. The number of samples per sub-stream in the three stages are $f_0 = 56$, $f_1 = 72$ and $f_2 = 63$ respectively. Further, each stage has $D = 2$, delay sub-streams. Thus, the total number of samples $M = 2 \sum_{i=0}^2 f_i = 382$. Note that the number of samples $M > 4k$ for this example. This is done intentionally for the illustrative purpose and to avoid the clutter in the figure. The figure shows a) the original 30-sparse spectrum \mathbf{X} . b) the spectrum estimated by the FFAST algorithm after 1 iteration. Note that it has correctly recovered 29 out of the 30 non-zero DFT coefficients. c) The FFAST algorithm recovers all the 30 non-zero DFT coefficients perfectly after 2 iterations.

this example. This is done intentionally for the illustrative purpose and to avoid the clutter in Fig. 13. Table V shows more empirical values of ℓ for different settings of the problem.

Probability of success: The empirical probability of success of the FFAST algorithm for the very-sparse as well as the less-sparse regimes is shown in Table V. We see that as long as the parameter η is above the minimum threshold η^* dictated by Table IV, in Section V-C1, the FFAST algorithm indeed computes all the non-zero DFT coefficients successfully with high probability. Further, in one or two instances when it failed to recover all the non-zero DFT coefficients, it has recovered all but 8 (for $d = 3$) or 16 (for $d = 4$) non-zero DFT coefficients. Thus, confirming our theoretical guarantees of recovering all but a vanishingly small fraction of the non-zero DFT coefficients with probability going

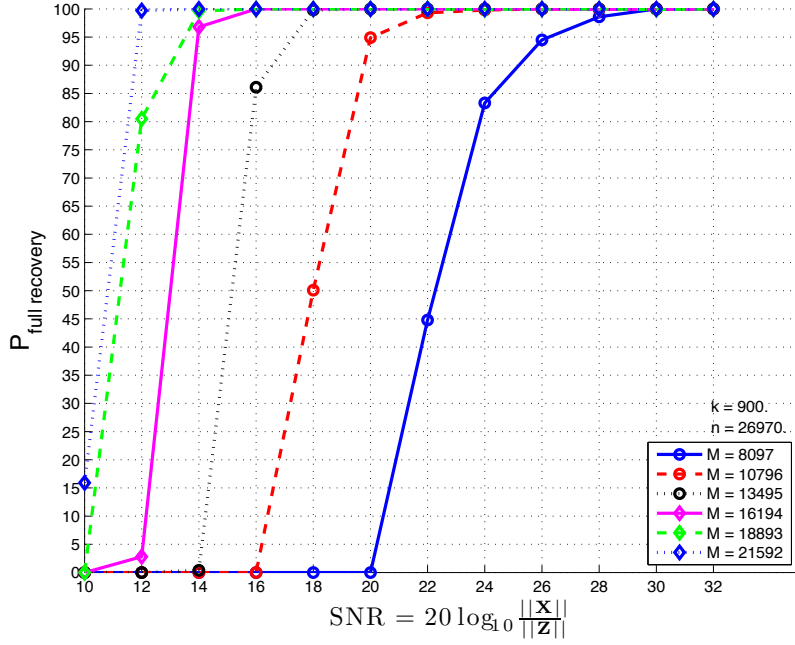


Fig. 14: Performance of the FFAST algorithm for computing the DFT of a signal \mathbf{x} that has an approximately sparse DFT. The approximately sparse DFT $\mathbf{X} = \mathbf{X}' + \mathbf{Z}$, where \mathbf{X}' is exactly k -sparse and \mathbf{Z} is an i.i.d zero mean unit variance Gaussian random vector. The non-zero coefficients of \mathbf{X}' take values in the set $\{\pm\sqrt{\rho}\}$, where the signal to noise ratio (SNR) is defined as $\text{SNR} = \mathbb{E}\{\|\mathbf{X}'\|_2^2 / \|\mathbf{Z}\|_2^2\} = k\rho/n$. The FFAST architecture consists of $d = 3$ stages, where $n = 26970$ and $k = 900$. The number of samples per sub-stream for each of the three stages in the FFAST front end architecture are set to $f_0 = 870, f_1 = 930$ and $f_2 = 899$ respectively. Further, each stage has D sub-streams, where we choose $D = 3, \dots, 8$. Thus, the total number of samples used by the FFAST algorithm are no more than $M = D \sum_{i=0}^2 f_i$. The decoding is successful if all the DFT coefficients are recovered perfectly. Each sample point in the plot is generated by averaging over 1000 runs. For example, when $D = 5$, the number of samples used by the FFAST algorithm are $M = 13495$, and it recovers all the DFT coefficients perfectly, with high probability, for all values of $\text{SNR} \geq 18\text{dB}$.

to one exponentially in k .

B. Performance of the FFAST algorithm for approximately k -sparse 1-D DFT signals

Although the theoretical claims in this paper are for exactly k -sparse signal \mathbf{x} , the FFAST algorithm is robust to the tail noise, i.e., approximately sparse signals, as well as to noisy observations. In this section we demonstrate the noise robustness of the FFAST algorithm empirically.

- The signal \mathbf{x} is of ambient dimension $n = 29 \times 30 \times 31 = 26970$, and the number of non-zero DFT coefficients $k = 900$. The FFAST architecture used for this simulation has $d = 3$ stages. The uniform sampling periods for the 3 stages are 31, 29, and 30. This results in the number of samples per sub-stream in the three stages to be $f_0 = 29 \times 30 = 870$, $f_1 = 30 \times 31 = 930$, and $f_2 = 31 \times 29 = 899$, respectively. Further, in each stage there are D sub-streams of the sub-sampled input data, where $D = 3, \dots, 8$. Note that, unlike the exact-sparse case, the number of sub-streams per stage for the approximately sparse setting is now *greater than two*. This results in increased sample complexity, $M = D \sum_{i=0}^2 f_i$. The additional samples are used for noise-robustness.
- For each run, an n -dimensional exactly k -sparse signal \mathbf{X}' is generated with non-zero values $X'_i \in \{\pm\sqrt{\rho}\}$, where ρ determines the SNR, and the positions of the non-zero coefficients are chosen to be uniformly at random in $\{0, \dots, n-1\}$. An n -length random vector \mathbf{Z} consisting of i.i.d $\mathcal{N}(0, 1)$ is generated and added to the exactly sparse \mathbf{X}' to get an approximately sparse signal $\mathbf{X} = \mathbf{X}' + \mathbf{Z}$.

The time domain signal \mathbf{x} is then obtained by taking the IDFT of \mathbf{X} . This discrete-time signal \mathbf{x} is then given as an input to our FFAST algorithm.

- Signal to noise ratio (SNR) is defined as $\text{SNR} = \mathbb{E}\{\|\mathbf{X}'\|_2^2 / \|\mathbf{Z}\|_2^2\} = k\rho/n$.
- Each sample point in Fig. 14 is generated by averaging over 1000 runs.
- Decoding is successful if all the DFT coefficients are recovered perfectly.

The performance of the FFAST algorithm for the Gaussian tail noise model is shown in Fig. 14. Note, for a fixed number of samples M , the FFAST algorithm shows a threshold behavior, i.e., there is a threshold SNR above which the FFAST algorithm recovers all the DFT coefficients perfectly. The threshold SNR after which the FFAST algorithm successfully decodes all the DFT coefficients decreases with increasing number of the samples as one would expect. While our analysis for the exactly sparse case requires $M < 4k$ samples for reconstruction, in the noisy case of approximately sparse signals, we end up taking more samples that in general depend on both k and n and also on the SNR and reliability requirements. An exact characterization of the increase in sample complexity as a function of SNR and reliability guarantees is part of our future work.

C. Empirical performance of the FFAST algorithm for 2-D DFT signals

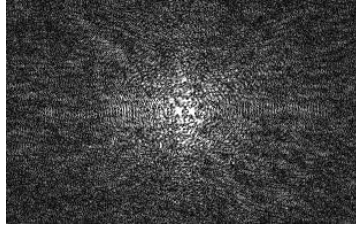
The 1-D FFAST architecture proposed in this paper can be generalized to a multi-dimensional DFT with similar sparsity guarantees for the exactly sparse case. As an example, in this section we demonstrate an application of the FFAST algorithm for 2-D images. One possible way to extend the FFAST architecture of Fig. 2 to 2-D signals is to consider a 2-D signal as a matrix of data, and subsample the data separably along the rows and the columns using a small set of uniform sampling pattern guided by the CRT. Specifically, we show here an application of the FFAST algorithm for a differential image in an Magnetic Resonance Imaging (MRI) for both the exactly k -sparse as well for an approximately k -sparse images. In MRI, the samples are acquired in the 2-D Fourier domain, and the difference images are sparse in the spatial domain. For example, the image shown in Fig. 15(b) is a difference image between two consecutive axial slices of brain image and is exactly sparse in the spatial domain. The FFAST algorithm acquires the Fourier samples from the spectral domain of the differential image shown in Fig. 15(a) and reconstructs the estimated image as shown in Fig. 15(c).

We provide simulation results for the 3 different types of images with parameters as specified below,

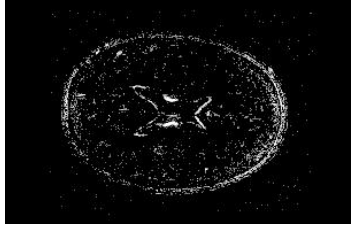
- **Brain Image:** The brain image shown in Fig. 15(b) is a difference between two consecutive axial slices of brain image and is exactly sparse in the spatial domain. The original image is 195×308 pixels, i.e., $n = 60060$. The FFAST algorithm samples the image in the 2-D Fourier domain, see Fig. 15(a), using a 3-stage FFAST architecture to get $M = 8910$ samples. The number of non-zero coefficients are $k = 3250$. The reconstructed image by the FFAST algorithm is shown in Fig. 15(c) which is identical to the original image.
- **Shepp-Logan Phantom Image:** The Shepp-Logan Phantom image shown in Fig. 15(e) is also of size 195×308 pixels, i.e., $n = 60060$, with exactly $k = 812$ non-zero pixels. The FFAST algorithm perfectly reconstructs the image as shown in Fig. 15(f) using $M = 8910$ samples.
- **‘Cal’ Image:** The ‘Cal’ image shown in Fig. 15(h) is a synthetic image of size 280×280 pixels, i.e., $n = 78400$. The spatial domain of the ‘cal’ image is approximately sparse with $k = 3509$ significant pixels and all other pixels take values from Gaussian $\mathcal{CN}(0, \sigma_z^2)$. The effective SNR is 16dB. The FFAST algorithm reconstructs the image shown in Fig. 15(i) using as few as $M = 10.06k = 35308$ Fourier samples. The reconstruction NMSE = 0.0085.

ACKNOWLEDGEMENTS

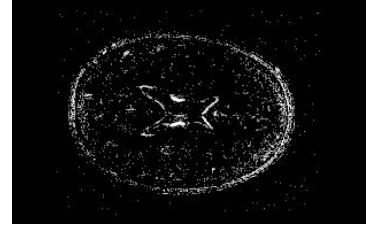
The authors would like to thank Frank Ong for providing the simulation results of 2D-DFT using the FFAST algorithm.



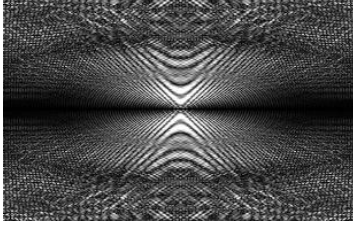
(a) 2-D Fourier transform of a difference image between two consecutive axial slices of Brain image.



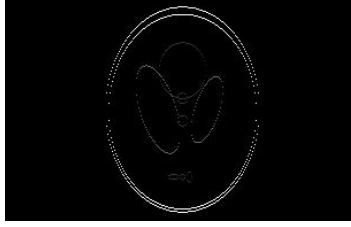
(b) Exactly $k = 3250$ sparse $n = 195 \times 308$ differential Brain image.



(c) Perfectly reconstructed image using the FFAST algorithm from $M = 2.74k = 8910$ samples.



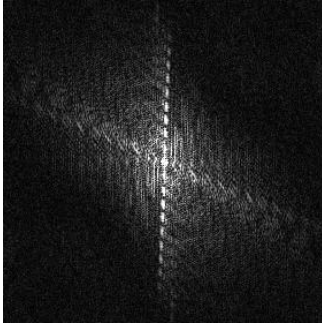
(d) 2-D Fourier transform of a Shepp-Logan Phantom Image.



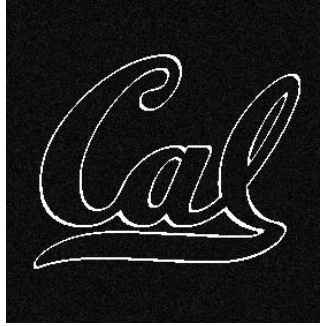
(e) Exactly $k = 812$ sparse $n = 195 \times 308$ Shepp-Logan Phantom spatial image.



(f) Perfectly reconstructed image using the FFAST algorithm from $M = 10.97k = 8910$ samples.



(g) 2-D Fourier transform of a noisy 'Cal' image.



(h) Approximately $k = 3509$ sparse (i.e. noisy) $n = 280 \times 280$ 'Cal' image. An exactly k sparse 2-D spatial 'Cal' image \mathbf{X}' is corrupted with 2-D i.i.d Gaussian noise \mathbf{Z} , with an effective SNR of 16dB, to obtain a noisy spatial domain 'Cal' image $\mathbf{X} = \mathbf{X}' + \mathbf{Z}$.



(i) Reconstructed image using the FFAST algorithm from $M = 10.06k = 35308$ samples.

Fig. 15: The figure shows the performance of the FFAST algorithm on the exactly-sparse differential brain image, the 'Shepp-Logan Phantom' image and an approximately sparse 'Cal' image. The Brain and Shepp-Logan phantom images are of size 195×308 pixels, i.e., $n = 60060$, with different levels of sparsity. The 'Cal' image is 280×280 and has sparsity $k = 3509$ in addition to the Gaussian tail noise of an effective SNR of 16dB.

APPENDIX

A. Edge degree-distribution polynomial for bins-and-balls model

The edge-degree distribution polynomial of a bi-partite graph is defined as $\rho(\alpha) = \sum_{i=1}^{\infty} \rho_i \alpha^{i-1}$, where ρ_i denotes the probability of an edge (or fraction of edges) of the graph is connected to a check node of degree i . Recall that in the randomized construction based on a balls-and-bins model described

in Section V-A, every variable node chooses one neighboring node in each of the d subsets of check nodes uniformly at random. Thus, the number of edges connected to a check node, in the subset with f_0 check nodes, is a binomial $B(1/f_0, k)$ random variable. So when k is large, the binomial distribution $B(1/f_0, k)$ is well approximated by a Poisson random variable with mean $1/\eta$. Thus,

$$Pr(\text{check node has edge degree} = i) \approx \frac{(1/\eta)^i e^{-1/\eta}}{i!}. \quad (13)$$

Let $\rho_{0,i}$ be the fraction of the edges, that are connected to a check node of degree i in set 0. Then, we have,

$$\begin{aligned} \rho_{0,i} &= \frac{if_0}{k} Pr(\text{check node has edge degree} = i) \\ &\stackrel{(a)}{\approx} \frac{if_0}{k} \frac{(1/\eta)^i e^{-1/\eta}}{i!} \\ &\stackrel{(b)}{\approx} \frac{(1/\eta)^{i-1} e^{-1/\eta}}{(i-1)!}, \end{aligned} \quad (14)$$

where (a) follows from Poisson approximation of the Binomial random variable and (b) from $f_0 = \eta k + O(1)$. Since, $f_i = \eta k + O(1)$ for all $i = 0, 1, \dots, d-1$. We have,

$$\rho_i \approx \frac{(1/\eta)^{i-1} e^{-1/\eta}}{(i-1)!} \quad (15)$$

and

$$\rho(\alpha) = e^{-(1-\alpha)/\eta} \quad (16)$$

B. Proof of Lemma 7

Proof: We provide a proof using a contradiction argument. If possible let S be the set of the variable nodes that the peeling-decoder fails to decode. We have $|S| \leq \alpha k$. Without loss of generality let $|N_1(S)| \geq |N_i(S)|$, $\forall i \in \{0, \dots, d-1\}$. Then, by the hypothesis of the Theorem $|N_1(S)| > |S|/2$.

Note that the peeling-decoder fails to decode the set S if and only if there are no more singleton check nodes in the neighborhood of S and in particular in $N_1(S)$. For all the check nodes in $N_1(S)$ to be multi-ton, the number of edges connecting to the check nodes in set $N_1(S)$ have to be at least $2|N_1(S)| > |S|$. This is a contradiction since there are only $|S|$ edges going from set S to $N_1(S)$ by construction. \blacksquare

C. Proof of Lemma 8

Proof: Consider a set S of variable (left) nodes in a random graph from the ensemble $\mathcal{C}_1^k(\mathcal{F}, m)$, where $|\mathcal{F}| = d \geq 3$. Let $N_i(S)$ be the right neighborhood of the set S in the i^{th} subset of check nodes, for $i = 0, 1, \dots, d-1$. Also, let E_S denote the event that the all the d right neighborhoods of S are of size $|S|/2$ or less, i.e., $\max\{|N_i(S)|\}_{i=0}^{d-1} \leq |S|/2$. First, we compute an upper bound on the probability

of the event E_S as follows:

$$\begin{aligned}
Pr(E_S) &< \prod_{i=0}^{d-1} \left(\frac{|S|}{2f_i} \right)^{|S|} \left(\frac{f_i}{|S|/2} \right) \\
&\stackrel{(a)}{\approx} \left(\frac{|S|}{2\mathbf{F}} \right)^{d|S|} \left(\frac{\mathbf{F}}{|S|/2} \right)^d \\
&< \left(\frac{|S|}{2\mathbf{F}} \right)^{d|S|} \left(\frac{2\mathbf{F}e}{|S|} \right)^{d|S|/2} \\
&< \left(\frac{|S|e}{2\mathbf{F}} \right)^{d|S|/2}
\end{aligned} \tag{17}$$

where the approximation (a) uses $f_i = \mathbf{F} + O(1)$ for all $i = 0, \dots, d-1$. Next, using a union bound, over all possible sets of size $|S|$, we get an upper bound on the probability of an event E , that there exists some set of variable nodes of size $|S|$, whose all the d right neighborhoods are of size $|S|/2$ or less.

$$\begin{aligned}
Pr(E) &< Pr(E_S) \binom{k}{|S|} \\
&< \left(\frac{|S|e}{2\mathbf{F}} \right)^{d|S|/2} \left(\frac{ke}{|S|} \right)^{|S|} \\
&\stackrel{(b)}{<} \left[\left(\frac{|S|}{\mathbf{F}} \right)^{d-2} \left(\frac{e}{2} \right)^d \left(\frac{e}{\eta} \right)^2 \right]^{|S|/2} \\
&< O((|S|/m)^{|S|/2})
\end{aligned} \tag{18}$$

where in (b) we used $\mathbf{F} = \eta k$ and in the last inequality we have used $d \geq 3$ and $m = O(\mathbf{F})$. Then, specializing the bound in (18) for $|S| = \alpha k$, for small enough $\alpha > 0$, and $|S| = o(k)$ we get,

- For $|S| = \alpha k$, for small enough $\alpha > 0$:

$$Pr(E) < e^{-\epsilon k \log(m/k)}, \text{ for some } \epsilon > 0 \tag{19}$$

- For $|S| = o(k)$:

$$Pr(E) < O(1/m) \tag{20}$$

■

D. Proof of Lemma 5

Proof: a) [Expected behavior] Consider decoding on a random graph in the ensemble $\mathcal{C}_1^k(\mathcal{F}, m)$. Let Z_i , $i = 0, \dots, kd-1$, be an indicator random variable that takes value 1 if the edge \vec{e}_i is not decoded after ℓ iterations of the peeling-decoder and 0 otherwise. Then by symmetry $\mathbb{E}[Z] = kd\mathbb{E}[Z_1]$. Next, we compute $\mathbb{E}[Z_1]$ as,

$$\begin{aligned}
\mathbb{E}[Z_1] &= \mathbb{E}[Z_1 \mid \mathcal{N}_{\vec{e}_1}^{2\ell} \text{ is tree-like}] Pr(\mathcal{N}_{\vec{e}_1}^{2\ell} \text{ is tree-like}) \\
&\quad + \mathbb{E}[Z_1 \mid \mathcal{N}_{\vec{e}_1}^{2\ell} \text{ is not tree-like}] Pr(\mathcal{N}_{\vec{e}_1}^{2\ell} \text{ is not tree-like}) \\
&\leq \mathbb{E}[Z_1 \mid \mathcal{N}_{\vec{e}_1}^{2\ell} \text{ is tree-like}] + Pr(\mathcal{N}_{\vec{e}_1}^{2\ell} \text{ is not tree-like}).
\end{aligned}$$

In Appendix E we show that $Pr(\mathcal{N}_{\vec{e}_1}^{2\ell} \text{ is not tree-like}) \leq \gamma/F$ for some positive constant γ . Also we have $\mathbb{E}[Z_1 \mid \mathcal{N}_{\vec{e}_1}^{2\ell} \text{ is tree-like}] = p_\ell$ by definition. Thus,

$$\mathbb{E}[Z] < kdp_\ell + \frac{d\gamma}{\eta}, \quad (21)$$

where we have used $F = \eta k$.

b) [Concentration] In this part, we want to show that the number of edges Z , that are not decoded at the end of ℓ iterations of the peeling-decoder, is highly concentrated around kdp_ℓ . There are two potential ways of an edge not being decoded after ℓ iterations: 1) the 2ℓ depth neighborhood of the edge is not tree-like or 2) the neighborhood is tree-like but the edge belongs to the fraction of edges that are not decoded after ℓ rounds (as per density evolution equation (6)). Let T be the number of edges, out of the total of kd , that have tree-like neighborhood of depth 2ℓ . Let $T' \subseteq T$, be the number of edges not decoded despite having tree-like neighborhood. Then from Appendix E we know,

$$\mathbb{E}[T] > kd(1 - \epsilon/4) \quad (22)$$

for any $\epsilon > 0$. Moreover, from equation (6)

$$\mathbb{E}[T'] = Tp_\ell. \quad (23)$$

Next, we obtain a concentration result for T , by using the (now) standard argument of exposing the k variable nodes v_j , $j = 1, \dots, k$, (and hence the edges in the graph) one by one to set up a Doob's martingale and applying Azuma's inequality. In particular, let $Y_i = \mathbb{E}[T \mid v_1^i]$ be the expected value of T after exposing i variable nodes. Then, $Y_0 = \mathbb{E}[T]$ and $Y_k = T$ and the sequence Y_i forms a Doob martingale.

Now, consider any pair of graphs (determined by the choice of variable nodes) that differ only on $(i+1)^{th}$ variable node. The number of edges with tree-like neighborhood of depth 2ℓ in these graphs differ at most by a constant number, since the differing variable node can influence the 2ℓ depth neighborhood of only constant number of edges (since the left edge degree d is a constant). Hence, $|Y_{i+1} - Y_i| < c_i$, for some constant $c_i \forall i = 0, \dots, k-1$. Hence, using Azuma's inequality along with (22), we get,

$$Pr(kd - T > \epsilon kd/2) < \exp(-\beta_1 \epsilon^2 k), \quad (24)$$

for some constant β_1 that depends on the left degree d and constant η . Using Azuma's inequality the following concentration result for T' holds,

$$Pr(|T' - Tp_\ell| > \epsilon kd/2) < 2 \exp(-\beta_2 \epsilon^2 k). \quad (25)$$

The assertion then follows from (24), (25) and $T' \leq Z \leq T' + |kd - T|$. ■

E. Probability of Tree-like Neighborhood

Consider an edge \vec{e} in a randomly chosen graph $\mathcal{G} \in \mathcal{C}_1^k(\mathcal{F}, m)$. Next, we show that the neighborhood $\mathcal{N}_{\vec{e}}^{2\ell^*}$ of \vec{e} is tree-like with high probability, for any fixed ℓ^* . Towards that end, we first assume that the neighborhood $\mathcal{N}_{\vec{e}}^{2\ell}$ of depth 2ℓ , where $\ell < \ell^*$, is tree-like and show that it remains to be tree-like when extended to depth $2\ell+1$ w.h.p. Let $C_{\ell,i}$ be the number of check nodes, from set i , and M_ℓ be the number of variable nodes, present in $\mathcal{N}_{\vec{e}}^{2\ell}$. Also assume that t more edges from the leaf variable nodes in $\mathcal{N}_{\vec{e}}^{2\ell}$ to the check nodes at depth $2\ell+1$ are revealed without creating a loop. Then, the probability that the next revealed edge from a leaf variable node to a check node (say in set i) does not create a loop is $\frac{f_i - C_{\ell,i} - t}{f_i - C_{\ell,i}} \geq 1 - \frac{C_{\ell^*,i}}{f_i - C_{\ell^*,i}}$. Thus, the probability that $\mathcal{N}_{\vec{e}}^{2\ell+1}$ is tree-like, given $\mathcal{N}_{\vec{e}}^{2\ell}$ is tree-like, is lower bounded by $\min_i (1 - \frac{C_{\ell^*,i}}{f_i - C_{\ell^*,i}})^{C_{\ell+1,i} - C_{\ell,i}}$. Similarly assume that $\mathcal{N}_{\vec{e}}^{2\ell+1}$ is tree-like and s more edges from check nodes to the variable nodes at depth $2\ell+2$ are revealed without creating a loop.

Note the probability that a check node has degree ≥ 2 is upper bounded by k/\mathbf{F} and conditioned on the event that a check node has an outgoing edge it has equal chance of connecting to any of the edges of the variable nodes that are not yet connected to any check node. Thus, the probability of revealing a loop creating edge from a check node to a variable node at depth $2\ell + 2$ is upper bounded by, $(k/\mathbf{F})(1 - \frac{(k-M_{\ell^*}-s)d}{kd-M_{\ell^*}d-s}) \leq \frac{kM_{\ell^*}}{\mathbf{F}(k-M_{\ell^*})}$. Thus, the probability that $\mathcal{N}_{\vec{e}}^{2\ell+2}$ is tree-like given $\mathcal{N}_{\vec{e}}^{2\ell+1}$ is tree-like is lower bounded by $(1 - \frac{kM_{\ell^*}}{\mathbf{F}(k-M_{\ell^*})})^{M_{\ell+1}-M_{\ell}}$.

It now follows that the probability that $\mathcal{N}_{\vec{e}}^{2\ell^*}$ is tree-like is lower bounded by

$$\min_i \left(1 - \frac{kM_{\ell^*}}{\mathbf{F}(k-M_{\ell^*})}\right)^{M_{\ell^*}} \left(1 - \frac{C_{\ell^*,i}}{f_i - C_{\ell^*,i}}\right)^{C_{\ell^*,i}}$$

Hence, for k sufficiently large and fixed ℓ^* ,

$$\Pr(\mathcal{N}_{\vec{e}}^{2\ell^*} \text{ not tree-like}) \leq \max_i \frac{M_{\ell^*}^2}{\mathbf{F}} + \frac{C_{\ell^*,i}^2}{f_i} \leq \frac{\gamma}{\mathbf{F}}$$

for some constant $\gamma > 0$, since for any fixed value of ℓ^* , $C_{\ell^*,i}$ and M_{ℓ^*} are constant w.h.p and $f_i = \mathbf{F} + O(1)$ for all $i = 0, \dots, d-1$.

REFERENCES

- [1] D. Donoho, "Compressed sensing," *Information Theory, IEEE Transactions on*, vol. 52, no. 4, pp. 1289–1306, 2006.
- [2] E. Candes and T. Tao, "Near-optimal signal recovery from random projections: Universal encoding strategies?" *Information Theory, IEEE Transactions on*, vol. 52, no. 12, pp. 5406–5425, 2006.
- [3] K. Do Ba, P. Indyk, E. Price, and D. P. Woodruff, "Lower bounds for sparse recovery," in *Proceedings of the Twenty-First Annual ACM-SIAM Symposium on Discrete Algorithms*. Society for Industrial and Applied Mathematics, 2010, pp. 1190–1197.
- [4] E. Price and D. P. Woodruff, "(1+ eps)-approximate sparse recovery," in *Foundations of Computer Science (FOCS), 2011 IEEE 52nd Annual Symposium on*. IEEE, 2011, pp. 295–304.
- [5] C. Temperton, "Self-sorting mixed-radix fast fourier transforms," *Journal of computational physics*, vol. 52, no. 1, pp. 1–23, 1983.
- [6] R. Gallager, "Low-density parity-check codes," *Information Theory, IRE Transactions on*, vol. 8, no. 1, pp. 21–28, 1962.
- [7] J. W. Byers, M. Luby, M. Mitzenmacher, and A. Rege, "A digital fountain approach to reliable distribution of bulk data," in *ACM SIGCOMM Computer Communication Review*, vol. 28, no. 4. ACM, 1998, pp. 56–67.
- [8] M. Luby, "Digital fountain, inc. luby@digitalfountain.com," 2002.
- [9] M. Luby and M. Mitzenmacher, "Verification codes: simple low-density parity-check codes for large alphabets," in *Proc. 40th Annu. Allerton Conf. Communication, Control, and Computing*. Citeseer, 2002, pp. 38–47.
- [10] R. Prony, "Essai experimental,-," *J. de l'Ecole Polytechnique (Paris)*, vol. 1, no. 2, pp. 24–76, 1795.
- [11] V. F. Pisarenko, "The retrieval of harmonics from a covariance function," *Geophysical Journal of the Royal Astronomical Society*, vol. 33, no. 3, pp. 347–366, 1973.
- [12] R. Schmidt, "Multiple emitter location and signal parameter estimation," *Antennas and Propagation, IEEE Transactions on*, vol. 34, no. 3, pp. 276–280, 1986.
- [13] R. Roy and T. Kailath, "Esprit-estimation of signal parameters via rotational invariance techniques," *Acoustics, Speech and Signal Processing, IEEE Transactions on*, vol. 37, no. 7, pp. 984–995, 1989.
- [14] E. Candès, J. Romberg, and T. Tao, "Robust uncertainty principles: Exact signal reconstruction from highly incomplete frequency information," *Information Theory, IEEE Transactions on*, vol. 52, no. 2, pp. 489–509, 2006.
- [15] J. Tropp and A. Gilbert, "Signal recovery from random measurements via orthogonal matching pursuit," *Information Theory, IEEE Transactions on*, vol. 53, no. 12, pp. 4655–4666, 2007.
- [16] M. Vetterli, P. Marziliano, and T. Blu, "Sampling signals with finite rate of innovation," *Signal Processing, IEEE Transactions on*, vol. 50, no. 6, pp. 1417–1428, 2002.
- [17] P. Dragotti, M. Vetterli, and T. Blu, "Sampling moments and reconstructing signals of finite rate of innovation: Shannon meets strang-fix," *Signal Processing, IEEE Transactions on*, vol. 55, no. 5, pp. 1741–1757, 2007.
- [18] T. Blu, P. Dragotti, M. Vetterli, P. Marziliano, and L. Coulot, "Sparse sampling of signal innovations," *Signal Processing Magazine, IEEE*, vol. 25, no. 2, pp. 31–40, 2008.
- [19] M. Mishali and Y. Eldar, "From theory to practice: Sub-nyquist sampling of sparse wideband analog signals," *Selected Topics in Signal Processing, IEEE Journal of*, vol. 4, no. 2, pp. 375–391, 2010.
- [20] A. C. Gilbert, S. Guha, P. Indyk, S. Muthukrishnan, and M. Strauss, "Near-optimal sparse fourier representations via sampling," in *Proceedings of the thirty-fourth annual ACM symposium on Theory of computing*, ser. STOC '02. New York, NY, USA: ACM, 2002, pp. 152–161. [Online]. Available: <http://doi.acm.org/10.1145/509907.509933>
- [21] A. C. Gilbert, S. Muthukrishnan, and M. Strauss, "Improved time bounds for near-optimal sparse fourier representations," in *Proc. SPIE Wavelets XI*, 2003.
- [22] A. C. Gilbert, M. J. Strauss, and J. A. Tropp, "A tutorial on fast fourier sampling," *Signal Processing Magazine, IEEE*, vol. 25, no. 2, pp. 57–66, 2008.

- [23] H. Hassanieh, P. Indyk, D. Katabi, and E. Price, “Nearly optimal sparse fourier transform,” in *Proceedings of the 44th symposium on Theory of Computing*. ACM, 2012, pp. 563–578.
- [24] —, “Simple and practical algorithm for sparse fourier transform,” in *Proceedings of the Twenty-Third Annual ACM-SIAM Symposium on Discrete Algorithms*. SIAM, 2012, pp. 1183–1194.
- [25] M. Iwen, A. Gilbert, and M. Strauss, “Empirical evaluation of a sub-linear time sparse dft algorithm,” *Communications in Mathematical Sciences*, vol. 5, no. 4, pp. 981–998, 2007.
- [26] B. Ghazi, H. Hassanieh, P. Indyk, D. Katabi, E. Price, and L. Shi, “Sample-optimal average-case sparse fourier transform in two dimensions,” *arXiv preprint arXiv:1303.1209*, 2013.
- [27] M. Iwen, “Combinatorial sublinear-time fourier algorithms,” *Foundations of Computational Mathematics*, vol. 10, no. 3, pp. 303–338, 2010.
- [28] R. Blahut, *Fast algorithms for digital signal processing*. Addison-Wesley Longman Publishing Co., Inc., 1985.
- [29] S. Pawar and K. Ramchandran, “A hybrid dft-ldpc framework for fast, efficient and robust compressive sensing,” in *Proceedings of the 50th Allerton*, 2012.
- [30] S. Kay, “A fast and accurate single frequency estimator,” *Acoustics, Speech and Signal Processing, IEEE Transactions on*, vol. 37, no. 12, pp. 1987–1990, 1989.
- [31] M. Luby, M. Mitzenmacher, M. Shokrollahi, and D. Spielman, “Improved low-density parity-check codes using irregular graphs,” *Information Theory, IEEE Transactions on*, vol. 47, no. 2, pp. 585–598, 2001.
- [32] T. Richardson and R. Urbanke, “The capacity of low-density parity-check codes under message-passing decoding,” *Information Theory, IEEE Transactions on*, vol. 47, no. 2, pp. 599–618, 2001.
- [33] M. Mitzenmacher and E. Upfal, *Probability and computing: Randomized algorithms and probabilistic analysis*. Cambridge University Press, 2005.
- [34] M. Luby, M. Mitzenmacher, M. Shokrollahi, and D. Spielman, “Efficient erasure correcting codes,” *Information Theory, IEEE Transactions on*, vol. 47, no. 2, pp. 569–584, 2001.